TECHNICAL RESEARCH REPORT

SYSTEMS RESEARCH CENTER

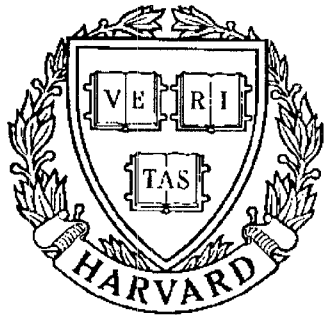

Supported by the National Science Foundation Engineering Research Center Program (NSFD CD 8803012), Industry and the University

Receptive Field Organization in Ferret Primary Auditory Cortex: Spectral Orientation Columns

by S. Shamma, J.W. Fleshman and P.R. Wiser

TR 90-46

Receptive Field Organization in Ferret Primary Auditory Cortex: Spectral Orientation Columns

Shihab A. Shamma[a], *James W. Fleshman*[b], *and Philip R. Wiser*[c]

(a) Electrical Engineering Department, University of Maryland Institute for Advanced Computer Studies, and Systems Research Center. University of Maryland, College Park, MD 20742. The Mathematical Research Branch, NIDDDK, National Institutes of Health, Bethesda, MD 20892.

(b) Systems Research Center, University of Maryland, College Park, MD 20742. *Present Address:* National Center for Biotechnology Information, National Library of Medicine, Bethesda, MD 20894.

(c) Electrical Engineering Department, University of Maryland, College Park, MD 20742.

Running Head: Organization of Primary Auditory Cortex

Mailing Address: Shihab Shamma, Electrical Engineering Department, University of Maryland, College Park. MD. 20742.

Telephone numbers: (301) 454-6867 (Office), (301) 454-6942 (Lab).

SUMMARY AND CONCLUSIONS

1. We studied the topographic organization of the receptive fields obtained from single and multiunit recordings along the isofrequency planes of the primary auditory cortex (AI) in the barbiturate-anesthetized ferret.

2. Using a two-tone stimulus and bandlimited noise, the excitatory and inhibitory portions of the receptive field of each cell were determined and then parameterized in terms of a *symmetry index*. The index measures the net balance of excitatory and inhibitory influences around the best frequency (BF) of the cell.

3. The distribution of the symmetry index values along the isofrequency planes revealed systematic changes in the symmetry of the receptive fields. At the center, units with narrow and symmetric inhibitory sidebands predominated. These gave way gradually to asymmetric inhibition, with high frequencies (relative to the units' BFs) becoming more effective caudally, and low frequencies more effective rostrally. These response types tend to organize along one or more bands that parallel the tonotopic axis (i.e., orthogonal to the isofrequency planes).

4. Cell responses to spectrally shaped noise were consistent with the symmetry of their receptive fields. For instance, cells with strong inhibition from above the BF were most responsive to stimuli that contain least spectral energy above the BF, i.e., stimuli with the opposite asymmetry. In six animals, it was demonstrated that the spectral gradient (or "orientation") of the most effective stimulus varies systematically along the isofrequency planes.

5. In five animals, the selectivity of unit responses to the direction of a frequency-modulated (FM) tone was tested and found to correlate strongly with the symmetry index of the receptive fields. Specifically, cells with strong inhibition from frequencies above (below) the BF prefer increasing (decreasing) sweeps. Thus, selectivity to FM direction is also mapped along the isofrequency planes of the AI.

6. One functional implication of the receptive field organization is that cortical responses encode the locally averaged *gradient* of the acoustic spectrum by their differential distribution along the isofrequency planes. This enhances the representation of such features as the symmetry (or "orientation") of spectral peaks, edges, and the spectral envelope. This scheme,

together with FM selectivity, can be viewed as the one dimensional analogue of the orientation columns and direction of motion selectivity of the visual cortex.

INTRODUCTION

The mammalian primary auditory cortex, AI, plays an important role in localizing and processing complex sounds [5,9,14,27,56]. Despite extensive neurophysiological and anatomical study, the organizational principles underlying cortical auditory function, and the primitives that the cortex employs to represent sound remain poorly understood. Only two organizational principles have been identified in AI: first, frequency is mapped in an orderly fashion across the surface of AI (the tonotopic axis) [17,22,23,33]; second, cells with similar responses to binaural stimuli tend to occupy irregular bands that are oriented parallel to the tonotopic axis and, therefore, approximately orthogonal to the isofrequency contours [13,24]. These superimposed tonotopic and binaural response maps are analogous to the retinotopic map and the ocular dominance columns of the visual cortex [12]. In the visual cortex maps have also been found for other image attributes such as selectivity to edge orientations and direction of motion [12,58]. Corresponding ordered representations of complex spectral or temporal attributes of sound (e.g. spatial maps, amplitude- or frequency-modulation, or elements of species-vocalizations) have not been identified in the primary auditory cortex [1,2,7,25,41,53,55,57]. Recent data from cat's primary auditory cortex, however, have suggested a possible organization of FM responses along the isofrequency planes [21].

The aim of this study was to determine whether features of the acoustic spectrum other than frequency and laterality are represented topographically across the ferret AI cortex. Our approach was to avoid making an *a priori* guess as to what acoustic features would be important. Instead, we examined a more general response property of cortical cells, namely the organization of their excitatory and inhibitory receptive fields[1]. Our specific goal was to establish whether

[1]The term *receptive field* of a cell is used here to denote its response as a function of frequency *at a particular intensity*. In a linear system, it would be called the *transfer function*. Since cortical cell responses do change with sound level, receptive fields are usually measured at several intensities.

systematic changes occur in these receptive fields as a function of position along the isofrequency contours. If so, then it may be possible to determine what spectral features of the stimulus those changes represented and their functional significance. Preliminary findings were published as abstracts in [10,46].

METHODS

Young adult ferrets (approximately 1 kg) were anesthetized with sodium pentobarbital (40 mg/kg, ip) and given 0.1 mg/kg Atropine sc. An areflexic level of anesthesia was maintained throughout the surgical preparation and subsequent neural recording session by continuous iv infusion of pentobarbital (approximately 5 mg/kg/hr) diluted with dextrose-electrolyte solution to maintain the animal hydration and to provide nourishment. In our experience, nutrition during the experiment was essential to keeping the animals alive and in good condition for prolonged recording periods (24 hours). A tracheal cannula was inserted and breathing was unassisted. Body temperature was maintained near 37°C using a heating pad and blankets. The ectosylvian gyrus, which includes the primary auditory cortex [16,17], was exposed by craniotomy and the overlying dura was incised and reflected. The brain was covered in 2% agar in saline to reduce pulsations. The contralateral pinna and most of the fleshy meatus were resected. The ear canal was cleaned, and a speculum containing a Sony MDR-E464 miniature speaker was sutured to the meatal stump. Single unit action potentials and spikes from multicell clusters were recorded using tungsten-in-glass microelectrodes.

Pure tone stimuli (single-tone, two-tone, and FM) were generated using two independent function generators, gated and mixed, and then fed through a common equalizer into the earphones. Before gating and delivery, noise stimuli were spectrally shaped by an independent computer-controlled equalizer (1/3 octave resolution). Calibration of the sound delivery system (up to 20kHz) was performed *in situ* prior to each experiment using a 1/8 inch B&K probe microphone (type 4170). The microphone was inserted into the ear canal to within 5 mm of the tympanic membrane.

Responses were usually evoked by one or two pure tone bursts (200 ms duration, 10 ms rise- and fall-times, 0–50 ms intertone delay), frequency modulated tones, or noise bursts.

Parameters of the test stimuli are described later in the text. Neural signals were led through a window discriminator and the time of spikes occurrence relative to stimulus delivery was stored using a Hewlett-Packard 9000/800 series minicomputer. The computer also controlled stimulus delivery, and created raster displays and spike count histograms of the responses.

For each animal, our strategy was to maximize the number of penetrations obtained along one isofrequency plane, and to record if possible from more than one such plane. This necessarily limited the number of stimulus parameters tested in a given penetration. In all experiments, we have aimed consistently to record at a depth of 350-600 μm where the excitatory phasic responses to single tones were strongest. Histological examination of Nissl-stained sections showed that this depth corresponds to cortical layers III and IV in young adult ferrets.

An experiment typically consisted of 10–40 useful microelectrode penetrations spaced 100–300 μm apart. In each penetration, 1–5 cells or cell clusters were studied. In a few cases, we have recorded responses at various depths to measure the variation of the responses. The frequency range tested in a given animal was often dictated by the available cortical surface not obstructed by superficial blood vessels.

For each cell or cell cluster, we first determined the best frequency manually, followed by a tuning curve with 1/8 octave resolution. Determining the BF accurately was important, especially in cases where the tuning was broad at the moderate sound intensities used in the two-tone tests. An experiment was concluded with an overdose of pentobarbital after 12-24 hours of recordings.

RESULTS

The Tonotopic Organization of the Ferret Auditory Cortex

In order to outline the extent and borders of the primary auditory cortex (AI) in the ferret and its location relative to other auditory fields, we carried out experiments to map in detail the tonotopic organization of the different auditory fields. Responses from different regions can be roughly organized based on a combination of factors: The sharpness of tuning, the overall tonotopic order, and the strength and nature of the time course of the response (e.g., response

latency and whether the response is phasic or sustained). Figure.1 illustrates the typical cortical organization that emerged from maps obtained in 18 animals. We also illustrate in this figure rasters of the unit responses that characterize the some of the different cortical areas.

The results can be summarized by comparison with the cat's auditory cortex. There are two tonotopic maps that correspond to the AI and the anterior auditory field (AAF). Four additional fields exist that may correspond to the secondary auditory cortex (AII) and other cortical fields of the cat [10]. Only AI responses have been previously described in the ferret [16,17].

Responses to single tones in AI are similar to those described in the cat in that they are strong, non-adaptive, sharply tuned, and have a short latency (15-20 ms) [2,30]. Low frequencies are represented laterally, and high frequencies medially. Frequency tuning becomes broader and the responses weaker towards the edges of AI. Frequencies represented range from 100 Hz to over 35 kHz, with the best responses near 5-8 kHz. The exact location of AI on the ectosylvian gyrus, and particularly its width, varied from one animal to another. On average, AI occupies the dorsomedial-most 3-4 mm of the ectosylvian gyrus, extending into the supra-sylvian fissure. AI becomes wider in the high BF regions (width 1-2 mm for low BFs, 3-4 mm for high BFs).

On the rostro-medial edge of AI, BFs approach 20-25 kHz and then reverse their upward trend and begin to decrease rapidly in the areas located within the bank of the sulcus. This putative anterior auditory field (AAF) extends along the deep walls of the supra-sylvian fissure for 1-2 mm, with a reversed tonotopic map that seems to emphasize the representation of the low frequencies (<12 kHz). The responses here are quite similar to those in AI with sharp tuning and short-latencies.

Lateral to AI, a belt of cortex extends caudally from the psuedo-sylvian fissure to the supra-sylvian fissure. Its responses are distinguished from AI by their broad tuning, adaptability to repeated tone bursts, higher thresholds, and relatively long latencies (>20 ms). No clear tonotopic organization can be discerned here because of the broad tuning curves. This field may correspond to the AII field of the cat [16].

Three other smaller fields can be readily identified, although their correspondence to the cat's cortical fields is unclear. First, a broadly tuned area (B) is found lateral to the AI-AAF

latency and whether the response is phasic or sustained). Figure.1 illustrates the typical cortical organization that emerged from maps obtained in 18 animals. We also illustrate in this figure rasters of the unit responses that characterize the some of the different cortical areas.

The results can be summarized by comparison with the cat's auditory cortex. There are two tonotopic maps that correspond to the AI and the anterior auditory field (AAF). Four additional fields exist that may correspond to the secondary auditory cortex (AII) and other cortical fields of the cat [10]. Only AI responses have been previously described in the ferret [16,17].

Responses to single tones in AI are similar to those described in the cat in that they are strong, non-adaptive, sharply tuned, and have a short latency (15-20 ms) [2,30]. Low frequencies are represented laterally, and high frequencies medially. Frequency tuning becomes broader and the responses weaker towards the edges of AI. Frequencies represented range from 100 Hz to over 35 kHz, with the best responses near 5-8 kHz. The exact location of AI on the ectosylvian gyrus, and particularly its width, varied from one animal to another. On average, AI occupies the dorsomedial-most 3-4 mm of the ectosylvian gyrus, extending into the supra-sylvian fissure. AI becomes wider in the high BF regions (width 1-2 mm for low BFs, 3-4 mm for high BFs).

On the rostro-medial edge of AI, BFs approach 20-25 kHz and then reverse their upward trend and begin to decrease rapidly in the areas located within the bank of the sulcus. This putative anterior auditory field (AAF) extends along the deep walls of the supra-sylvian fissure for 1-2 mm, with a reversed tonotopic map that seems to emphasize the representation of the low frequencies (<12 kHz). The responses here are quite similar to those in AI with sharp tuning and short-latencies.

Lateral to AI, a belt of cortex extends caudally from the psuedo-sylvian fissure to the supra-sylvian fissure. Its responses are distinguished from AI by their broad tuning, adaptability to repeated tone bursts, higher thresholds, and relatively long latencies (>20 ms). No clear tonotopic organization can be discerned here because of the broad tuning curves. This field may correspond to the AII field of the cat [16].

Three other smaller fields can be readily identified, although their correspondence to the cat's cortical fields is unclear. First, a broadly tuned area (B) is found lateral to the AI-AAF

border, with vigorous, short latency, responses to single tones. Second, a small area (M) of very low frequencies is located deep in the cusp of the supra-sylvian fissure. The transition from the very high BFs (>30 kHz) of AI to low BFs (<1 kHz) is quite sudden and striking. Third, a relatively large belt of cortex (C) borders the caudal edge of AI and extends along and into the supra-sylvian fissure. Responses here are relatively broad and generally similar to those of AII. Nevertheless, a tonotopic order can be discerned with increasing BFs away from AI (i.e., roughly reversed map).

All responses described in the remainder of this report were obtained in AI. As is the case for the cat and other mammals, the general location of AI in relation to the supra-sylvian fissure is unambiguous, although the exact orientation and position of the tonotopic map may vary. This variation can be seen for 17 ferrets in the maps of Figs. 9-14. Therefore, it was generally necessary during the mapping experiments to make several initial penetrations to ascertain the orientation of AI. The physiological criteria by which the ferret AI responses are recognized are quite distinctive: sharp tuning, low thresholds, large evoked potentials, short-latency, phasic but non-adaptive responses, and precise tonotopic organization.

The Two-Tone Stimulus: Three Response Types and the Symmetry of the Receptive Fields

The principal acoustic stimulus used in this study was the two-tone stimulus. It consisted of two tone pips of equal duration with staggered onset times (as illustrated in Fig. 2A). The first tone ($T1$) was presented at several frequencies centered around the best frequency (BF) of the cell. $T1$ defines the limits of the excitatory portion of the receptive field (see Fig. 2B). Because of the depression of spontaneous activity (a well-known effect of the anesthetic used in these experiments [6,29]), it was difficult to see the inhibitory portions of the receptive field using a single tone. To overcome this problem, a second tone ($T2$) was fixed at BF, with a delay of 0–50 ms relative to $T1$, to provide a level of background activity against which inhibitory $T1$ effects could be detected.

Figures. 2-4 illustrate the raster responses from three typical cells and the response features of interest in this study. In Fig 2, the unit is sharply tuned (BF = 8.5 kHz), responding to the excitatory tone ($T1$) over a narrow range of frequencies (< 1/2 octave; solid curve in

Fig. 2B). The $T1$ tone suppresses the response to $T2$ over a broader range on either side of BF (approximately 6–12 kHz; dashed curve in Fig. 2B). Two regions of $T2$ suppression are distinguished : frequencies where $T1$ excites the cell, i.e., within the narrow tuning curve of the cell; and frequencies where $T1$ elicits little or no response, i.e., the so-called *side-bands* of the tuning curve. Within the side-bands, the suppression of the BF response is presumably due to active inhibition originating from other units tuned to the side-band frequencies. This side-band or *lateral* inhibition has been observed in all central auditory nuclei [3,20,26,34,36,45,51], as well as in other sensory systems [11,32]. The suppression of the phasic $T2$ response at BF could result from a similar mechanism or may be a consequence of the adaptive or inhibitory mechanism that underlies the phasic response to $T1$ alone. This suppression appears to be proportional to the preceding excitation of the cell. Thus, it is maximal at BF where $T1$ is most excitatory, and weakens towards the edges of the excitatory response area. When no side-band inhibition is present, a gradual overlap of the $T1$ and $T2$ responses results in shallow or approximately flat total spike count over all frequencies (e.g., Figs. 5 and 9-13).

Figure. 3 illustrates a cell with a different pattern of inhibition. The cell is narrowly tuned at a BF of 8.0 kHz. However, in contrast to Fig. 2, the inhibition due to the T1 tone is nearly one-sided, being relatively strong above the BF, and weak below the BF. Therefore, the combined spike count curve (Fig. 3C) has a larger dip above the BF.

An example of a cell with an opposite asymmetry is shown in Fig. 4. Once again, the excitatory responses to T1 are well tuned ($BF = 3.5$ kHz). The inhibitory influences of T1 are stronger here below the BF; hence the combined spike count curve in Fig. 4C is asymmetric with a large dip below the BF.

In order to detect and measure the symmetry of the receptive fields along the isofrequency contours, we computed the following simple statistic for the net excitatory and inhibitory influences acting on a cell or cell cluster with a given BF:

$$M = \frac{R_{>BF} - R_{<BF}}{R_{>BF} + R_{<BF}}, \tag{1}$$

where $R_{>BF}$ and $R_{<BF}$ are the total number of spikes for all frequencies above and below the BF, respectively. Spikes are usually counted during an 80 ms time window following the onset

of the $T1$ tone. Thus, *unless stated otherwise*, the time window used in all counts in this report is the 100-180 ms interval along the time axis of the rasters shown. This window includes the phasic responses of both tones, as illustrated by the combined spike count curves in Figs. 2-4C. If the excitatory and inhibitory responses are approximately equal around BF, the measure (M) will be near zero. Inhibition of $T2$ responses by $T1$ stimuli above BF and/or spread of $T1$-excitation to lower frequencies ($< BF$) causes M to be negative. Conversely, stronger low frequency inhibition or high frequency $T1$ excitation produces positive M values.

Another measure of symmetry that produces very similar response maps is the location relative to the BF of the centroid (C) of the combined spike count curve. It is computed from the rasters as follows:

$$C = \sum_{i=-N}^{N} iR_i / \sum_{i=-N}^{N} R_i, \tag{2}$$

where N is the number of $T1$ frequency steps on either side of the BF, i is the integer index of these steps ($i = -N, -N+1, ..., 0$ (at BF),..., $N-1, N$), and R_i is the spike count at the i^{th} step. As with the M index, C is near zero for symmetric cells. It is negative (positive) for strong inhibition above (below) the BF. In this report, we used the M index to characterize all two-tone data, whereas the C index were used for the noise and FM stimuli.

To summarize, basic characteristics of the receptive fields of cortical cells can be described by an index of symmetry (M or C) that reflects the balance of inhibition and excitation around the BF of the cell. Based on the value of this index, three typical responses exist: symmetric responses with narrow side-band inhibition on both sides of the BF, and asymmetric responses with strong inhibition above or below the BF.

Response Variabilities

The three response types illustrated above in Figs. 2-4 are typical in that they resemble closely the average rasters computed from many cells across different animals. A significant range of variations, however, exists in the character of the responses observed within each of the three types. This is because computing the simple indices (M or C), while helpful in constructing the cortical maps and detecting response trends, cannot capture the rich variety of responses that were recorded (e.g., in Figs. 5-7).

Examples of four different symmetric responses are displayed in Fig. 5. In the top two rasters, the responses exhibit strong side-band inhibition. While this inhibition is typically narrow around the BF ($< \pm 1/2$ octave, as in Fig. 2), it may broaden considerably in some cells ($\geq \pm 1$ octave around the BF, as in the top rasters of Fig. 5). This often correlates with the well established general broadening of the tuning of the excitatory responses for cells of lower BFs (≤ 2.5 kHz) [30,37]. In many cases of symmetric responses, side-band inhibition is quite narrow or weak and hence more difficult to detect, as illustrated in the bottom row of rasters.

For the class of cells with negative M values, the responses exhibit varying spread of inhibition above the BF, and spread of excitation below it. In the top row of Fig. 6, more examples of the typical response of this class are illustrated for cells with different BFs. In all examples, both the excitatory and inhibitory responses are relatively compact, i.e., excitation $\leq \pm 1/2$ octave, and inhibition < 1 octave above the BF. The most common variation of these responses concerns the overall strength of the inhibition, as illustrated by the rasters in the middle row of Fig. 6. In the leftmost raster, the inhibition is profound over an octave above the BF. The rasters to the right show a progressive decrease in the extent and strength of the inhibition, and a tendency of the excitatory responses to spread considerably below the BF. These trends are also seen in the examples in the bottom row, where the inhibition again decreases in the rasters from left to right. Note that $T1$ in these rasters is presented at two intensities so as to highlight the spread of excitation that usually accompanies the weakening of the side-band inhibition above the BF.

Analogous variations for cells with positive indices are shown in Fig. 7. First, examples of the typical responses of this class are illustrated in the top row of Fig.7, where the inhibitory and excitatory fields are relatively compact. Variations in the strength and spread of inhibition are shown in the middle series of rasters. Finally, responses with two $T1$ intensities are illustrated in the bottom row, where it is evident that a spread of the excitatory responses may accompany the weakening inhibition (from left to right). However, this is less common than the spread to low frequencies seen earlier in Fig. 6.

This variability likely reflects the diversity of cortical cell types and morphologies throughout the different cortical layers. In order to maximize the uniformity of our records, we have restricted our recordings to a depth range of 350-600 μm which, as mentioned earlier, corresponds to layers III and IV in young adult ferrets. In a typical penetration, the first neural responses to a tone stimulus are phasic evoked potentials at tone onset and offset. These were often followed by cells with strong OFF responses at a depth of approximately 300 μm. Large phasic excitatory responses appear at around 350 μm. In our experience, these evoked potentials are a reliable physiological criterion of the desired depth. In addition, we have often opted to record from cell clusters rather than single cells in order to average out these potential sources of variability. Such manipulations are common in similar cortical mapping experiments [24,42].

A different source of variability in the symmetry indices is the choice of stimulus parameters, e.g., the inter-tone delays and relative intensity levels. Changing these parameters for a given cell affected somewhat the absolute values of the M or C index, but rarely changed the basic response characteristics (e.g., changing M from a large positive to large negative values, or vice versa). Fig. 8 illustrates the stability of the responses for two cells with decreasing inter-tone delays. In the top row the cell maintained a strong inhibition above the BF for all delays. In the bottom row, the inhibition was mostly below the BF.

The same observations hold for the choices of the intensity levels. As a rule, the intensity of the $T2$ (BF) tone was always chosen to provide an adequate background of responses against which inhibition could be detected (typically at 60–70 dB SPL). Since T1 tone levels need to exceed T2 to produce their effects, T1 was most often chosen at 5–20 dB SPL higher than T2 (65-80 dB SPL). Higher levels of T1 were avoided to ensure linearity of our acoustic delivery system. The most typical change that occurs when increasing the T1 level relative to T2 is for negative (positive) M values to become more negative (positive) (see for instance examples in Figs. 6-7). Changes of sign occur almost exclusively in the near symmetric penetrations [2].

[2] We emphasize here that the indices M or C for a given penetration are usually computed as the average of several tests per cell. It follows, therefore, that cells with large negative or positive indices are (by definition) those less sensitive to manipulations of stimulus parameters.

In order to maintain consistency throughout the experiments, we have chosen specific values of the stimulus parameters: inter-tone delay = 30 ms, and T1 intensity larger than T2 by 5–20 dB SPL. Finally, it should be noted that the random character of these and other sources of variability can only serve to obscure regular trends in the maps. Consequently, evidence of systematic organization in the distributions of the response is a testimony to the robustness of its underlying causes.

The topographic distribution of the M index

We examined the spatial distribution of receptive field asymmetry, as reflected in the M index, along the isofrequency contours of the primary auditory cortex in 23 animals. Representative maps are shown in Figs. 9-14. In Figs. 9-13 we illustrate rasters from closely spaced electrode penetrations that were made along isofrequency strips with various BFs. Fig.14 summarizes experiments from 12 other animals. The value of M in any given penetration represents the averaged value of all tests performed in the penetration, which may include recordings of 2 or 3 separate units or unit clusters.

A consistent finding in our experiments is a location dependent change in the values of the index, due largely to a change in the efficacy of the inhibitory side-bands along the isofrequency contours. Specifically, at the center of AI, the receptive fields typically possess a narrow excitatory region often flanked by narrow and symmetric inhibitory side-bands, as illustrated by the responses in Figs. 2 and 5 . In this region of AI, M is near zero ($\pm$ 0.07). In the maps of Figs. 9-14, penetrations with such intermediate M values are marked by the partially shaded circles. Moving caudally from the center of AI, the high frequency ($> BF$) inhibitory side-bands become broader and/or more potent than the low frequency side-bands ($< BF$). This is usually accompanied by a gradual broadening of the excitatory response area towards lower frequencies. The combined effect of these changes is to make the M values more negative ($<$ -0.07). Penetrations with these responses are indicated in the maps by clear circles.

Moving rostrally away from the center of AI, the opposite trends occur. Low frequency inhibition is strengthened relative to the high frequency side-bands. This is sometimes accompanied by a spread of the $T1$ excitatory responses to higher frequencies, although this is not as

common as the spread of excitation to low frequencies observed in more caudal penetrations. The combined effect of these trends is to increase the values of the M parameter (> 0.07). Penetrations characterized by these responses are indicated in the maps of Figs. 9-14 by black circles.

The distribution of the M values along the isofrequency planes spans all the frequencies we tested (0.5–11 kHz) in an orderly manner to give the appearance of continuous bands that run orthogonal to the isofrequency contours (e.g., maps of Figs 10-12). It is common in our experiments that a reversal in these trends occurs in the rostral and/or caudal areas of AI. See for instance the rasters spanning the transition regions in Fig. 12 (cells 74/08a03.t2 and 74/10a02.t2) and Fig. 13 (cells 47/21a02.t2, 47/22a02.t2, 47/24a02.t2). In all maps, we have marked with dashed lines the borders of the region where M changes *once* from extreme positive to extreme negative values. In general, we did not investigate in detail the regions outside these lines to establish reliably the existence or number of repeated bands. This was partly due to experiment time limitations, and partly because the responses outside the "main" band became weaker, and units more difficult to isolate.

Still further beyond the transition regions, the tuning of the excitatory responses broadens, and the responses may abruptly change to those typical of non-primary auditory fields (e.g., weaker, rapidly adapting responses, longer latencies, broad tuning [33,42]). Another reliable indicator of the borders of AI is the gradual weakening of the excitatory evoked responses elicited by single tones. There is, however, no obvious systematic increase in the threshold of responses of units that could be isolated. We have also recorded the rate-level functions of many cells along with their receptive fields. As expected, most non-monotonic cells have strong inhibitory fields [30,45]; however, no clear topographical segregation of such units can be discerned in our data.

Response Maps for Spectrally Shaped Noise Stimuli

In six animals, an additional stimulus paradigm was used to assess asymmetry in the receptive fields above and below BF. The stimuli were three spectrally shaped noise bursts (Fig.15A). One stimulus was narrowband ($< 2/3$ octaves) placed symmetrically about the BF

of the cell. The response to this stimulus provided the reference against which the responses to the other two asymmetric bands were compared. For each cell, the symmetry index, C, was computed from the responses as follows:

$$C = \frac{R_{>BF} - R_{<BF}}{R_{>BF} + R_{BF} + R_{<BF}} \tag{3}$$

where $R_{>BF}$, R_{BF}, $R_{<BF}$ are the response spike counts for each of the three noise bands, measured in the time window, 100–150 ms. Fig. 15B illustrates the correspondence between the shaped noise and two-tone raster responses from three types of cells. In the left rasters, the inhibition is below the BF, and hence the most effective noise stimulus is the one that has no energy below the BF (C=0.15). The opposite is true in the right rasters (C= -0.14). In the middle rasters, the sideband inhibition is apparently weak, and the responses are consequently stronger for the wide band stimuli (C=0.0). The topographic distributions of this index in 6 animals are shown in Fig. 16. Black (clear) circles represent penetrations excited best by the noise band $\geq BF$ ($\leq BF$). These maps exhibit the same trends seen earlier with the two-tone stimulus in the corresponding maps of Figs. 10 and 14.

Responses to Frequency-Modulated (FM) Tones

One possible consequence of the asymmetry in the receptive field of a cell is its selectivity to the direction of an FM stimulus. Such a property cannot be easily deduced from the two-tone and noise stimuli because of their pseudo-stationary nature. In order to test this hypothesis directly, FM tones were swept up and down past the BF of the cells, spanning a total frequency range of ± 1 octave, and presented at different rates (most often at 10, 30, and 50 KHz/sec; see bottom of Fig. 17A for an illustration of stimulus parameters). The symmetry of the average responses to the two sweep directions are assessed using the index C, with spike counts measured in a 100-150 ms time window for the up sweep ($R\uparrow$), and 375-425 ms for the down sweep ($R\downarrow$):

$$C = \frac{R\downarrow - R\uparrow}{R\downarrow + R\uparrow}. \tag{4}$$

FM stimuli were used in 5 experiments. In a total of 75 cells/clusters both FM and two-tone stimuli were tested and the response indices computed. In approximately 80% of all cells, there

is agreement between the response type of the two stimuli, i.e., cells with relatively strong inhibition above (below) the BF prefer upward (downward) sweeping tones. Symmetric cells respond well to both directions. Fig. 17B illustrates the two-tone and FM rasters of upward-, bidirectional-, and downward-sensitive cells (from left to right). The correspondence between the indices of the two tests suggests that FM selectivity is also mapped in a regular fashion along the isofrequency planes of AI. One such FM map is illustrated in Fig. 18A together with the FM rasters associated with each penetration. Two additional maps are shown in Fig. 18B.

FM stimuli were usually presented at several rates and in a few cases at several intensities. With a few exceptions that occur in the near symmetric cells, FM selectivity does not depend on rate or intensity. However, the strength of the responses does depend on the sweep rate. Some cells respond well only at fast rates (50 KHz/sec), while others only at slow or intermediate rates. No systematic trends, however, can be discerned from our data.

DISCUSSION

The data presented in this report suggest that there is an orderly change in the shape of the receptive fields along the rostro-caudal isofrequency contours of the ferret primary auditory cortex. In the center of AI, cells are sharply tuned with symmetric and narrow inhibitory sidebands, if any. Toward the edges of AI, the receptive fields become both *broad and asymmetric*, with high frequency ($> BF$) inhibition dominating caudally, and low frequency ($< BF$) inhibition dominating rostrally. These receptive field types form ordered (possibly repeating) bands that traverse the isofrequency planes orthogonally. Superimposed on this map is an orderly change in the responses to FM tones along the isofrequency planes. Cells with dominant inhibition from above (below) the BF respond selectively to upward (downward) frequency sweeps. At the center of AI, both directions are equally effective.

Gradual changes of *monaural* response properties along the isofrequency planes have been described previously, both in AI [21,39,42,47], in other cortical fields [41,42,48,49], and in precortical nuclei [28,35,38]. It is clear in our results that the balance of inhibitory inputs plays the critical role in shaping the symmetry of cortical receptive fields. The origin of this inhibition, however, is uncertain. The auditory cortex abounds with local inhibitory inter-neurons and

inputs [34,43,44] that may form the necessary substrate for these maps. Lateral inhibition, however, also exists at all other auditory nuclei. Consequently, it is uncertain whether the maps observed in these experiments are intrinsically cortical, or are manifestations of already formed maps at earlier centers (as is the case, for instance, for the binaural columns [54]).

From a functional point of view, there are two possible implications to this organization of the receptive fields. The first is that these receptive fields are directly responsible for the FM selectivity and its ordered mapping along the isofrequency planes. Similar, but not identical, maps have recently been detected in the cat's AI [21]. The correspondence between the receptive fields' asymmetry and the direction of FM selectivity demonstrated in this report has a direct analogue in the visual system where *motion direction* and *edge orientation* sensitivity are strongly correlated in the responses of the primary visual cortex.

This leads to the second functional interpretation of the results, that of encoding the acoustic spectrum in the distribution of cortical responses. The changing symmetry of the receptive fields along the isofrequency planes means that the responses along this axis will be differentially distributed according to the *local shape (or "orientation")* of the input spectrum at each frequency. This argument is clarified in the schematic diagrams of Fig. 19. For instance, for relatively narrow and symmetric spectral peaks (e.g., those due to low intensity single tones or a sharp resonance in a complex spectrum), all cells along the corresponding isofrequency planes will respond well since no inhibition is recruited from the side-bands (Fig. 19B). For skewed spectral peaks or spectral edges, the locus of the maximal response shifts away from the center towards cells with receptive fields of the opposite asymmetry, such that the input recruits the least inhibition. This model is schematically illustrated in Figs. 19C-D where the broadening of an input spectral peak towards higher frequencies causes a rostral shift in the maximal cortical response, since cells in caudal regions are more strongly inhibited above BF (Fig. 19C). The opposite shift occurs if the input peak is oriented towards lower frequencies (Fig. 19D).

Similar shifts may take place for broadband stimuli as illustrated in Figs. 19E-G. For instance, with a broad symmetric spectrum (e.g., white noise, Fig. 19E; or a strong peak flanked by balanced smaller peaks) the maximal response is centered since inhibition is most strongly

recruited by the asymmetric receptive fields near the edges of AI. The peak activity shifts rostrally when the spectral slope (or the envelope) tilts towards high frequencies (Figs. 19F), and caudally for the opposite tilt (Fig. 19G).

Therefore, the receptive field organization suggests a model in which the detailed shapes of spectral peaks and edges, and the shape of the global spectral envelope, are encoded in the two-dimensional distribution of neural activity across the extent of AI. A concise statement of the model, one that applies to all schematic responses described in Fig. 19, is that *the location of the maximal response along a particular iso-frequency plane encodes the locally smoothed gradient of the spectrum at that frequency.* This mapping scheme provides a neurophysiological basis for the significant role that spectral peaks and the spectral envelope are known to play in the perception and recognition of complex sounds. For instance, the envelope of the acoustic spectrum plays a dominant role in the perception of the timbre of complex sounds [31]. Furthermore, psychoacoustical studies have demonstrated that spectral features that can be enhanced with derivative operators (e.g., edges, peaks, and peak shoulders) are critical in the recognition of complex spectral patterns such as those of speech [4]. Finally, experiments on the perceptual distances between phonetic categories have revealed that the distance metrics that best correlate with perception are those based on spectral gradients, rather than on the spectrum itself [18].

These results have close parallels in the visual cortex where asymmetric receptive fields (in two-dimensional form) are common, and are thought to be involved in the production of ordered maps of orientation sensitivity [15]. This suggests a common organizational principle that unifies the primary auditory and visual cortical representations: *Both encode the locally smoothed gradients of their input patterns.* For the one dimensional world of auditory spectral inputs, this principle translates to the sensitivity to peak symmetries and spectral tilts. For the two dimensional world of visual images, it translates to the sensitivity to edge orientations. These arguments are in harmony with recent experimental results in which retinal cells of newborn ferrets were induced to project to the auditory thalamus and cortex [50]. Many cortical cells in the adult animal then exhibited visually driven responses, with oriented receptive fields

and other features typical of the visual cortex. A possible implication of these findings and of the auditory maps presented here is that the development of primary auditory and visual cortical maps may diverge largely because of the different nature of their inputs, rather than of their underlying functional principles.

Acknowledgement

This work is supported in part by grants from the Whitaker Foundation, the Naval Research Laboratory, and the Air Force Office of Scientific Research. We would also like to thank Jay Virdy and Preetham Gopalaswamy for their help in developing the data acquisition system.

References

[1] Abeles, M. and Goldstein, M.H. Jr. Functional architecture in cat primary auditory cortex: columnar organization and organization according to depth. *J. Neurophysiol.* 33: 172-187, 1970.

[2] Abeles, M. and Goldstein, M.H. Jr. Responses of single units in the primary auditory cortex of the cat to tones and to tone pairs. *Brain Res.* 42: 337-352, 1972.

[3] Aitken, L. and Dunlop, C. Inhibition in the medial geniculate body of the cat. *Exp. Brain Res.* 7: 68-63, 1969.

[4] Assmann P. and Summerfield Q. Modelling the perception of concurrent vowels: Vowels with the same fundamental frequency. *J. Acoust. Soc. Am.* 85: 327, 1988.

[5] Brugge, J.F., Dubrovsky, N.A., Aitkin, L.M. and Anderson, D.J. Sensitivity of single neurons in auditory cortex of cat to binaural tonal stimulation: Effects of varying interaural time and intensity. *J. Neurophysiol.* 32: 1005-1024, 1969.

[6] Brugge, J.F. and Merzenich, M.M. Responses of neurons in auditory cortex of the Macaque monkey to monaural and binaural stimulation. *J. Neurophysiol.* 36: 1138-1158, 1973.

[7] Brugge, J.F. and Reale, R.A. Auditory cortex. In *Cerebral Cortex. Volume 4: Association and auditory cortices.* Edited by A. Peters and E.G. Jones. New York: Plenum Press, 1985, pp. 229–271.

[8] Dickson, J.W. and Gerstein, G.L. Interactions between neurons in auditory cortex of the cat. *J. Neurophysiol.* 37: 1239-1261, 1974.

[9] Evans, E.F. and Whitfield, I.C. Classification of unit response in the auditory cortex of the unanaesthetized and unrestrained cat. *J. Physiol. (London)* 171: 476-493, 1964.

[10] Fleshman, J.W. and Shamma, S.A. Organization of the ferret auditory cortex. *Acoust. Soc. Am. Abstr.* S1, 84:56, Nov. 1988.

[11] Hartline H. K. *Studies on Excitation and Inhibition in the Retina.* Rockefeller University Press, 1974.

[12] Hubel D. and Wiesel T., Receptive Fields, binocular interaction and functional architecture in the cat's visual cortex, *J. Physiol. (London)* 160:106-154, 1962.

[13] Imig, T.J. and Adrian, H.O. Binaural columns in the primary field (AI) of cat auditory cortex. *Brain Res.* 138: 241-257, 1977.

[14] Jenkins, W.M. and Merzenich, M.M. Role of cat primary auditory cortex for sound-localization behavior. *J. Neurophysiol.* 52: 819-847, 1984.

[15] Jones, J. and Palmer, L., The Two-dimensional spatial structure of simple receptive fields in cat striate cortex. *J. Neurophysiol.* 58: 1187-1211, 1987.

[16] Kavanagh, G. and Kelly, J., Contribution of auditory cortex to sound localization by ferret *Mustela putorius. J. Neurophysiol.* 57: 1746-1766.

[17] Kelly, J., Judge, P., and Phillips, D., Representation of the cochlea in primary auditory cortex of the ferret *Mustela putorius. Hearing Res.* 24:111-115, 1986.

[18] Klatt, D. Prediction of perceived phonetic distance from critical-band spectra: A first step. *Proc. ICASSP* 82:1278, 1982.

[19] Marr, D. *Vision.* Freeman and Co., 1982.

[20] Martin, M. and Dickson, J. Lateral inhibition in the anteroventral cochlear nucleus of the cat: A microiontophoretic study. *Hearing Res.* 9: 35-41, 1983.

[21] Mendelson, J., Schreiner, C., Grasse, K., and Sutter, M. Spatial distribution of responses to FM sweeps in cat primary auditory cortex. *Proc.* 11^{th} *A.R.O. meeting*, pp.199, 1988.

[22] Merzenich, M.M., Kaas, J.H. and Roth, G.L. Auditory cortex in the grey squirrel: tonotopic organization and architectonic fields. *J. Comp. Neurol.* 166: 387-402, 1976.

[23] Merzenich, M.M., Knight, P.L. and Roth, G.L. Representation of cochlea within primary auditory cortex in the cat. *J. Neurophysiol.* 28: 231-249, 1975.

[24] Middlebrooks, J.C., Dykes, R.W. and Merzenich, M.M. Binaural response-specific bands in primary auditory cortex (AI) of the cat: Topographical organization orthogonal to isofrequency contours. *Brain Res.* 181: 31-48, 1980.

[25] Middlebrooks, J.C., Pettigrew, J.D. Functional classes of neurons in primary auditory cortex of the cat distinguished by sensitivity to sound location. *J. Neurosc.* 1:107-120, 1981.

[26] Moore, D., Semple, M., and Addison, P., Some acoustic properties of neurons in the ferret inferior colliculus. *Brain Res.* 269: 69-82, 1983.

[27] Neff, W., Diamond, W. and Casseday, J. Behavioral studies of auditory discrimination: Central nervous system. In: *Handbook of Sensory Physiology, Vol. 2.* Edited by W. Keidel and W. Neff. Berlin: Springer-Verlag, 1975, pp. 307-400.

[28] Palmer A. and King A. The representation of auditory space in the mammalian superior colliculus. *Science* 249-250, 1982.

[29] Pfingst, B.E. and O'Connor, T.A. Characteristics of neurons in auditory cortex of monkeys performing a simple auditory task. *J. Neurophysiol.* 45: 16-34, 1981.

[30] Phillips, D.P., Ormand, S.S., Musicant, A.D. and Wilson, G.F. Neurons in the cat's primary auditory cortex distinguished by their responses to tones and wide-spectrum noise. *Hearing Res.* 18: 73-86, 1985.

[31] Plomp, R. *Aspects of Tone Sensation*, 1976.

[32] Rall, W., Shepherd, G., and Reese, T. Dendro-dendritic synaptic pathway for inhibition in the olfactory bulb. *Exp. Neurol.* 14:44-56, 1966.

[33] Reale, R.A. and Imig, T.J. Tonotopic organization of auditory cortex in the cat. *J. Comp. Neurol.* 192: 265-291, 1980.

[34] Ribaupierre F., Goldstein M., Yani-komshian G. Intracellular study of the cat's primary auditory cortex, *Brain Res.*, 48: 185-204, 1972.

[35] Rodrigues-Dagaeff, C., Simm, G., De Ribaupierre, Y., Villa, A., De Ribaupierre, F., and Rouiller, E. Functional organization of the ventral division of the medial geniculate body of the cat: Evidence for a rostro-caudal gradient of response properties and cortical projections. *Hearing Res.* 39: 103-126, 1989.

[36] Sachs, M., Sinnott, J., and Heinz, R. Behavioral and physiological studies of hearing in birds. *Fed. Proc.* 37: 2329-2335, 1978.

[37] Sally, S. and Kelly, J. Organization of auditory cortex in the albino rat: Sound frequency. *J. Neurophysiol.* 59: 1627-1638, 1988.

[38] Schreiner C. and Langner G. Periodicity coding in the inferior colliculus of the cat. II. Topographical organization. *J. Neurophysiol.* 60: 1823-1840.

[39] Schreiner, C., Mendelson, J., Grasse, K., and Sutter, M., Spatial distribution of basic response properties in cat primary auditory cortex. *Proc.* 11^{th} *A.R.O. meeting*, pp.198, 1988.

[40] Schreiner, C. and Urbas, J. Representation of amplitude modulation in the auditory cortex of the cat. I. Anterior auditory field. *Hearing Res.* 21: 227-241, 1986.

[41] Schreiner, C. and Urbas, J. Representation of amplitude modulation in the auditory cortex of the cat. II. Comparison between fields. *Hearing Res.* 32: 49-64, 1988.

[42] Schreiner, C. and Cynader, M. Basic functional organization of second auditory cortical field (AII) of the cat. *J. Neurophysiol.* 51: 1284-1305, 1984.

[43] Serkov, F. and Yanouskii, E. Postsynaptic potentials of neurons of the cat auditory cortex. *Neurofiziologiya* 3: 339-349, 1971.

[44] Serkov, F. and Yanouskii, E. Characteristics of cortical inhibitory neurons. *Neurofiziologiya* 6: 119-126, 1974.

[45] Shamma, S.A. and Symmes, D. Patterns of inhibition in auditory cortical cells in awake squirrel monkeys. *Hearing Res.* 19: 1-13, 1985.

[46] Shamma, S. and Fleshman, J. Spectral orientation columns in the primary auditory cortex. *Proc.* 13^{th} *A.R.O. meeting*, 1990.

[47] Suga, N. Amplitude spectrum representation in the Doppler-shifted-CF processing area of the auditory cortex of the mustache bat. *Science* 196: 64-67, 1977.

[48] Suga, N. The extent to which biosonar information is represented in the bat auditory cortex. In *Dynamic Aspects of Neocortical function*, edited by G.M. Edleman, W.E. Gall, and W.M. Cowan. New York:Wiley, 1984, p.315-373.

[49] Suga, N. Analysis of frequency-modulated sounds by auditory neurons of echo locating bats. *J. Physiol. (London)* 179: 26-53, 1965.

[50] Sur, M., Garraghty, P., and Roe, A. Experimentally induced visual projections into auditory thalamus and cortex. *Science*, 242:1437–1441, 1988.

[51] Voight, H.F. and Young, E.D. Evidence of inhibitory interactions between neurons in the dorsal cochlear nucleus. *J. Neurophysiol.* 44: 76-96, 1980.

[52] Voight, H.F. and Young, E.D. Stimulus dependent neural correlation: an example from the cochlear nucleus. *Exp. Brain Res.* 60: 594-598, 1985.

[53] Watanabe, T. and Katsuki, Y. Response patterns of single auditory neurons of the cat to species-specific vocalization. *Jpn. J. Physiol.* 24: 135-155, 1974.

[54] Wenstrup, J., Ross, L., and Pollak, G. Binaural response organization within a frequency band representation of the inferior colliculus: implications for sound localization. *J. Neurosc.* 6:962-973, 1986.

[55] Whitfield, I. and Evans, E., Responses of auditory cortical neuron to stimuli of changing frequency. *J. Neurophysiol.* 28: 655-672, 1965

[56] Whitfield, I. Auditory cortex and the pitch of complex tones. *J. Acoust. Soc. Am.*, 67: 644-647, 1980.

[57] Winter, P. and Funkenstein, H.H. The effect of species-specific vocalization on discharge of auditory cortical cells in the awake squirrel monkey. *Exp. Brain Res.* 18: 489-504, 1973.

[58] Zeki, S. and Shipp, S. The functional logic of cortical connections, *Nature* 335: 311-317, 1988.

Figure Legends:

Figure 1

Tonotopic organization of the ferret auditory cortex. The solid arc represents the dorso-medial tip of the supra-sylvian fissure. Indicated are the iso-frequency lines in the primary auditory area (AI). The three rasters to the right are from single cells in this region exhibiting sharp tuning and tonotopic order. The anterior field (AAF) extends down the sulcus rostral to AI. The four rasters to the left are recorded from cells at progressively deeper locations down the sulcus (electrode penetration marked by the dot). Note the gradual decrease in the BF. Also indicated is the secondary auditory field (AII) with one response raster from the marked penetration. Three other regions are labeled: The broadly tuned area (B), the medial area (M), and the caudal area (C). The (M)edial and (R)ostral directions are indicated by the arrows; the arrow lengths represent 1 mm distances on the surface of the cortex.

Figure 2

Typical responses of a cell with symmetric side-band inhibition.

Fig. 2A: Raster of responses to a *two-tone* stimulus. The cell's BF is 8.5 kHz. $T1$ starts at 100 ms into the sweep; its intensity is indicated to the right of the raster (65 dB SPL); its frequency spans ± 2 octaves around the BF in 1/4 octave steps. Please note that here, as in all other rasters in this paper, the frequencies are labeled only to one significant place after the decimal in order not to crowd the figures. In reality, however, frequencies were determined and presented at better than 99.999% accuracy. The second tone, $T2$, is delayed by 30 ms relative to $T1$; frequency = BF; intensity = 60 dB SPL. Ten repetitions are made at each $T1$ frequency.

The phasic responses of the cell to the two tones are segregated because of the inter-tone delay. $T1$ responses start approximately 16 ms following the onset of the tone (i.e., at 116 ms), and are restricted to a narrow range of frequencies around the BF (8 kHz). $T2$ responses start at 144 ms. They are vigorous when $T1$ is not near BF and are suppressed otherwise. Lateral inhibition is evidenced by the near absence of responses to either tone at the frequencies marked by the two arrows.

Fig. 2B: Spike counts as a function of $T1$ frequency. **Solid curve** is the excitatory onset

response of $T1$ counted over a 30 ms window (100–135 ms); **dashed curve** is the response to the onset of $T2$, counted over a 20 ms window (135–150 ms).

Fig. 2C: The total spike count as a function of $T1$ frequency; the window is 80 ms long (100–180 ms).

Figure 3

Typical responses of a cell with asymmetric inhibition from above the BF.

Fig.3A: Same display features as in Fig.2A. The arrow marks the frequency of the one-sided inhibition.

Figs.3B-C: Same display features as in Figs.2B-C.

Figure 4

Typical responses of a cell with asymmetric inhibition from below the BF.

Fig.4A: Same display features as in Fig.2A. The arrow marks the frequency of the one-sided inhibition.

Figs.4B-C: Same display features as in Figs.2B-C.

Figure 5

Examples of the variability of responses from symmetric cells. In each raster, the $T1$ frequencies span $\pm$ 2 octaves around the BF, at 1/4 octave resolution; its intensity is indicated to the right of the raster. The plot in the right inset figure is of the *combined spike count curve* computed in the time window 100-180 ms (i.e., exactly as in Fig.2C except plotted sideways against the same frequency axis of the raster). The value of the index M computed from this plot is shown in the bottom left corner of each raster. *Top row* illustrates responses with strong side-band inhibition. *Bottom row* illustrates responses with weak or very narrow side-band inhibition.

Figure 6

Examples of the variability of responses from cells with asymmetric inhibition from above the BF. Rasters are as in Fig.5. *Top row* illustrates typical responses of this class of cells. Tests here span $\pm$2 octaves around the BF, at 1/4 octave resolution. *Middle row* illustrates cells with decreasing inhibition to the right. *Bottom row* displays rasters with two $T1$ intensities.

Note the spread of $T1$ excitatory responses with intensity as inhibition weakens from right to left.

Figure 7

Examples of the variability of responses from cells with asymmetric inhibition from below the BF. Rasters are as in Fig.5. *Top row* illustrates typical responses of this class of cells. *Middle row* illustrates cells with decreasing inhibition from right to left. *Bottom row* displays rasters with two $T1$ intensities. Note the spread of $T1$ excitatory responses with intensity as inhibition weakens from right to left. All rasters span ± 1 octave range around the BF.

Figure 8

Stability of two-tone responses with respect to changes in inter-tone delays. *Top row* inter-tone delays: 30,15,0 ms. *Bottom row* inter-tone delays: 50,20,0 ms.

Figure 9

The distribution of the *two-tone* response symmetry measure, M, in the ferret primary auditory cortex (# 54). The circles indicate the locations of the electrode penetrations along the isofrequency contours (shown schematically as solid straight lines); asterisks mark penetrations with weak auditory responses. The arc in each map represents the location of the supra-sylvian fissure; the dashed lines delineate the approximate borders of the band within which the M measure changes from extreme negative (clear circles) to extreme positive values (black circles). A key for the shading scheme used is shown on the left of the figure. The (M)edial and (R)ostral directions are indicated by the arrows; the arrow lengths represent 1/2 mm distances on the surface of the cortex. The rasters shown are those of cells sampled in the penetrations indicated by the arrows. **Please note that, in this map and all following maps, the M values given in the raster may infrequently disagree with that given by the shading of its penetration since the latter is an average value of all cells in the penetration.**

Figure 10

Same as Fig.9 but for ferret (# 65).

Figure 11

Same as Fig.9 but for ferret (# 73).

Figure 12

Same as Fig.9 but for ferret (# 74).

Figure 13

Same as Fig.9 but for ferret (# 47). Note that the upper row of rasters are recorded from the middle row of penetrations in the map.

Figure 14

Maps of the distribution of M values in the AI of 12 additional ferrets. Details are as in Fig. 9 map.

Figure 15

Fig. 15A: Responses to two-tone (top) and spectrally shaped noise (bottom) stimuli. Schematic spectra of the three noise stimuli used to measure the symmetry of AI receptive fields are shown to the left of the bottom raster. The numbers to the left of the bottom raster indicate the left/right slopes of the noise spectrum around the BF. The narrow-band stimulus is the most effective since side-band inhibition is strong (C=0.03).

Fig. 15B: Correspondence between the responses to the two-tone and noise stimuli in three different types of cells. Bottom rasters are as in Fig 15A. The index C values are (from left to right): 0.14, 0.0, -0.13.

Figure 16

Maps of the distribution of C values in AI using noise stimuli. All map features are similar to those of Fig.9. The 6 maps are from animals also tested with two-tone stimuli and whose maps are shown in Figs. 10 and 14.

Figure 17

Fig.17A: Responses to two tone (upper raster) and FM stimuli (lower rasters). The parameters of the FM stimulus are illustrated below the figure. Tones were swept either linearly or at an exponentially increasing rate, i.e., keeping a constant rate along the approximately logarithmic tonotopic axis. Both types of sweeps produce essentially similar responses. The trajectory of the frequency values in each 500 ms trial is shown below the figure. The frequency is first swept upwards from an octave below BF to an octave above it; it is maintained at $2BF$

for a short period, and then swept downwards in the opposite direction. For all rates (indicated by the numbers to the left of the raster), the stimulus is designed such that the BF is always traversed at the same times into the trial ($\approx$ 125 ms for the upward sweep, and $\approx$ 400 ms for the downward sweep). For this cell, both the two-tone and FM responses indicate asymmetric inhibition from above the BF.

Fig.17B: Correspondence between the two-tone (upper rasters) and FM (lower rasters) responses for three response types. In the left column, the cell is strongly inhibited from above the BF, and is selectively responsive to upward sweeps. The opposite case is shown in the right column. The middle cell is relatively symmetric.

Figure 18

Fig.18A: A map of the topographic distribution of FM responses in AI. Map features and symbols are as in Fig.9. Black (clear) circles mark penetrations with selective responses to downward (upward) sweeps. Shaded penetrations are less selective.

Fig.18B: Two additional maps of FM response selectivity.

Figure 19

Model of the receptive fields in AI and their responses to oriented spectral features. All schematic responses are based on analytical derivations and computer simulations of a model of AI with gradually changing receptive fields along the iso-frequency planes.

Fig. 19A: The receptive fields along the isofrequency contours of AI. The vertical dimension represents the tonotopic axis of AI, with low frequencies (lf) at the bottom and high frequencies at the top (hf); the horizontal dimension represents the (R)ostro-(C)audal axis of the iso-frequency planes. The center receptive field is symmetric, with narrow excitatory fields and tight side-band inhibition (shaded portions of the receptive field). To the right (caudally), inhibition from higher frequencies predominates, and the excitatory field spreads to lower frequencies; the opposite occurs to the left (rostrally).

Fig. 19B: The response pattern elicited by a narrow spectral peak (e.g., a low intensity tone). Darker shading indicates stronger responses. All cells along the iso-frequency plane are well excited, and the response pattern is therefore symmetric relative to this axis.

Fig. 19C: The response pattern elicited by a spectral peak oriented towards higher frequencies. Caudal receptive fields recruit more inhibition, thus becoming weakly driven. Rostral receptive fields recruit more excitation causing the region of maximal response to shift rostrally.

Fig. 19D: The response patterns to a low frequency oriented spectral peak. The region of maximal responses shifts caudally as more inhibition is recruited by rostral receptive fields.

Fig. 19E: The response patterns to a flat spectrum. Only a limited frequency range is illustrated. The region of maximal responses is centered with respect to the iso-frequency plane since strong inhibition is recruited by the receptive fields at the edges.

Fig. 19F: The response patterns to a broad spectrum oriented towards high frequencies. The responses are illustrated only for a limited frequency range. The region of maximal responses shifts rostrally since caudal receptive fields recruit stronger high frequency inhibition becoming weakly driven. The opposite occurs in the rostral fields.

Fig. 19G: The response patterns to a broad spectrum oriented towards low frequencies. The responses are illustrated only for a limited frequency range. The region of maximal responses shifts caudally since rostral fields recruit stronger low frequency inhibition becoming weakly driven.

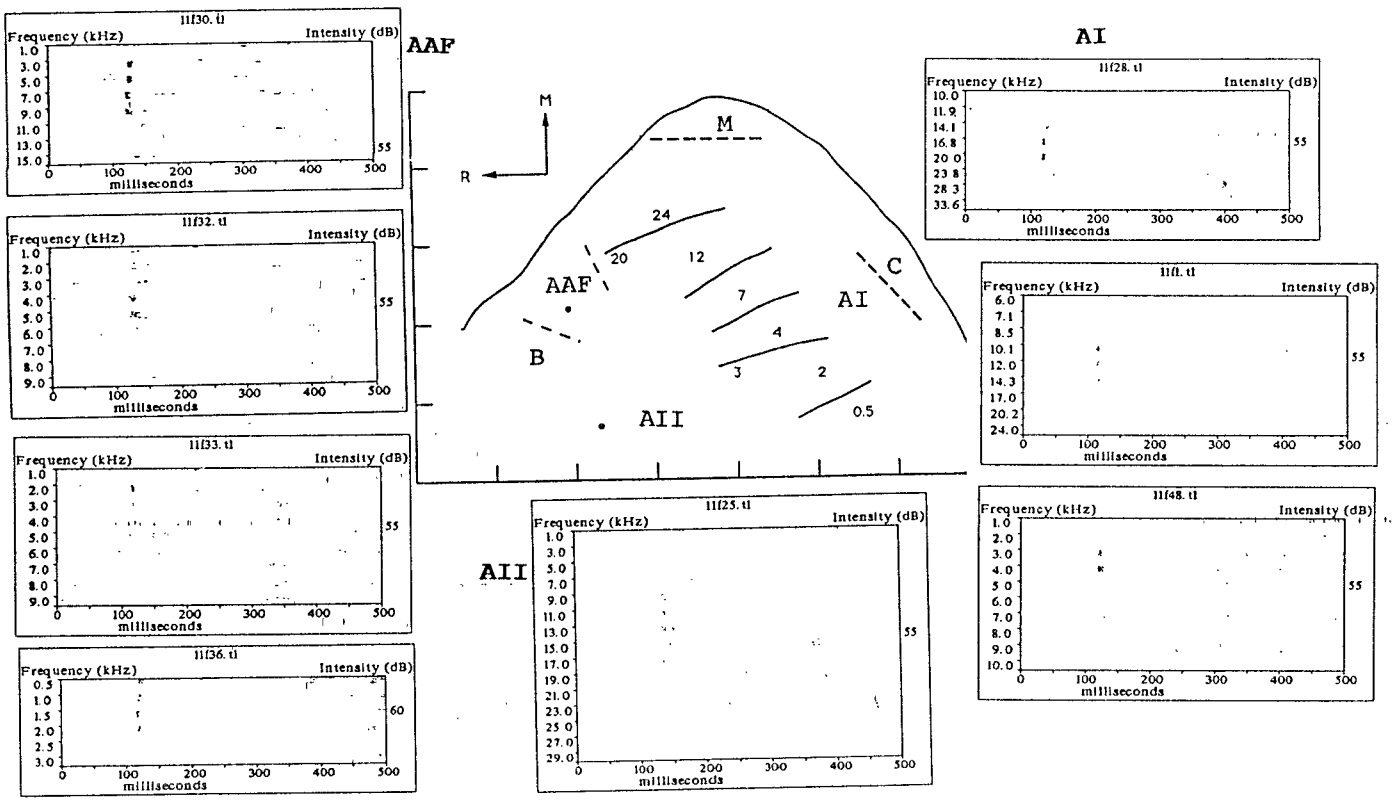
AAF
AI
AII
M
R
24
20
12
7
4
3
2
0.5
B
C
11f30.tl
11f32.tl
11f33.tl
11f36.tl
11f28.tl
11ft.tl
11f48.tl
11f25.tl
Frequency (kHz)
Intensity (dB)
milliseconds

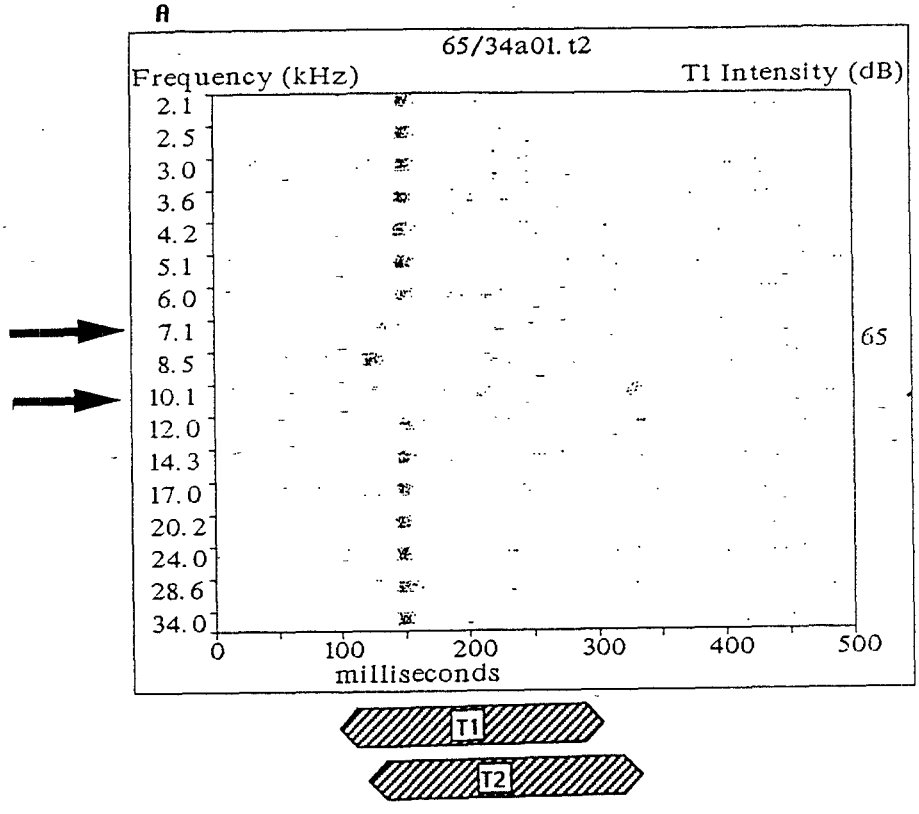
A
65/34a01.t2
Frequency (kHz)
T1 Intensity (dB)
2.1
2.5
3.0
3.6
4.2
5.1
6.0
7.1
8.5
10.1
12.0
14.3
17.0
20.2
24.0
28.6
34.0
65
0
100
200
300
400
500
milliseconds
T1
T2

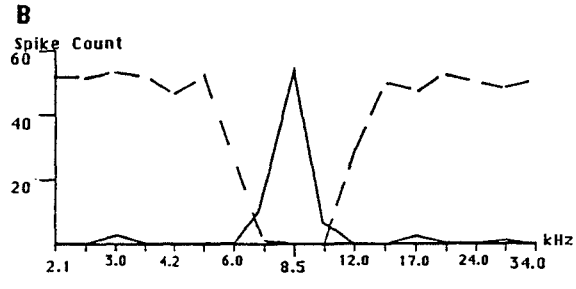
B
Spike Count
60
40
20
kHz
2.1
3.0
4.2
6.0
8.5
12.0
17.0
24.0
34.0

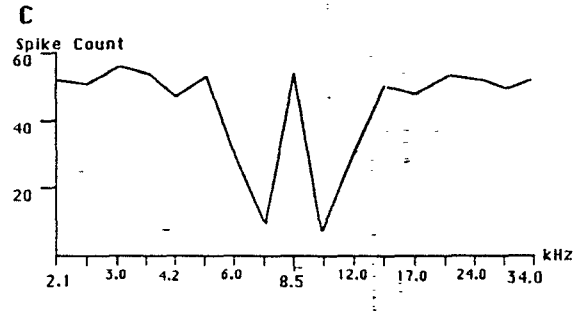
C
Spike Count
60
40
20
kHz
2.1
3.0
4.2
6.0
8.5
12.0
17.0
24.0
34.0

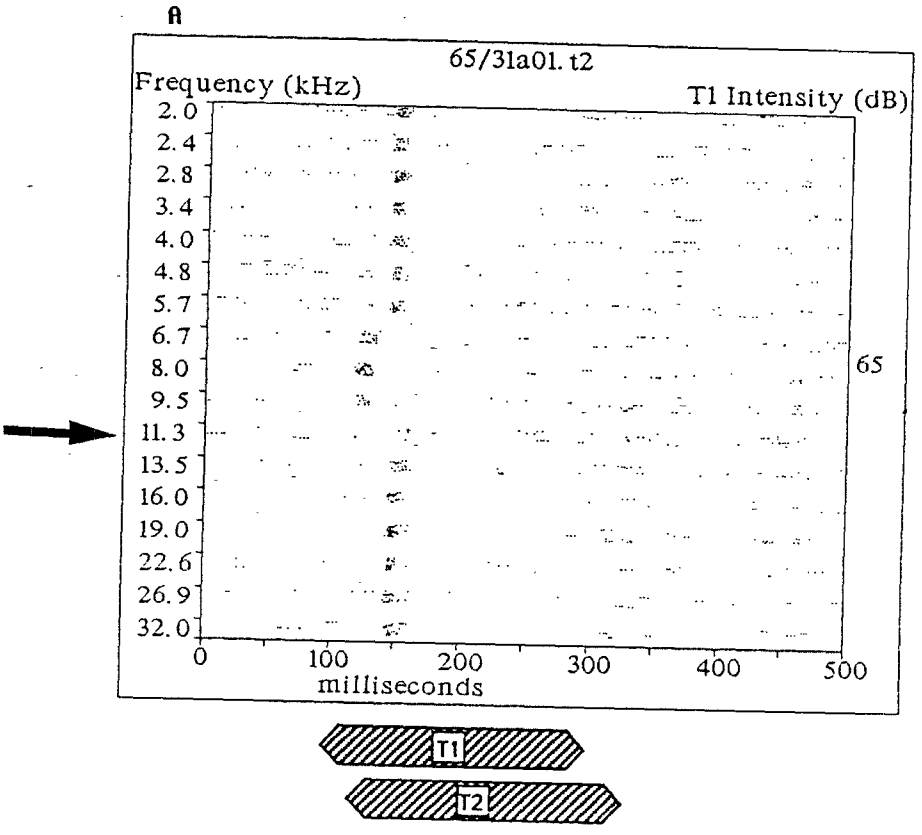
A
65/31a01.t2
Frequency (kHz)
T1 Intensity (dB)
2.0
2.4
2.8
3.4
4.0
4.8
5.7
6.7
8.0
9.5
11.3
13.5
16.0
19.0
22.6
26.9
32.0
65
0
100
200
300
400
500
milliseconds
T1
T2

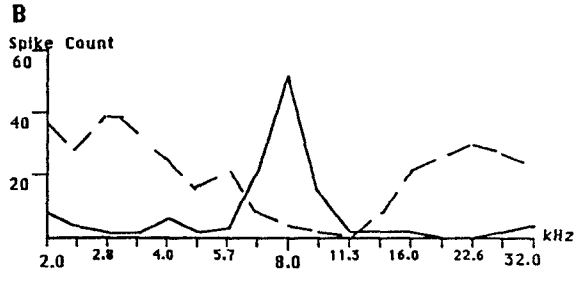
B
Spike Count
60
40
20
kHz
2.0
2.8
4.0
5.7
8.0
11.3
16.0
22.6
32.0

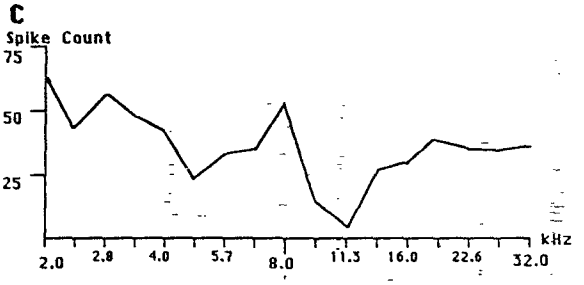
C
Spike Count
75
50
25
kHz
2.0
2.8
4.0
5.7
8.0
11.3
16.0
22.6
32.0

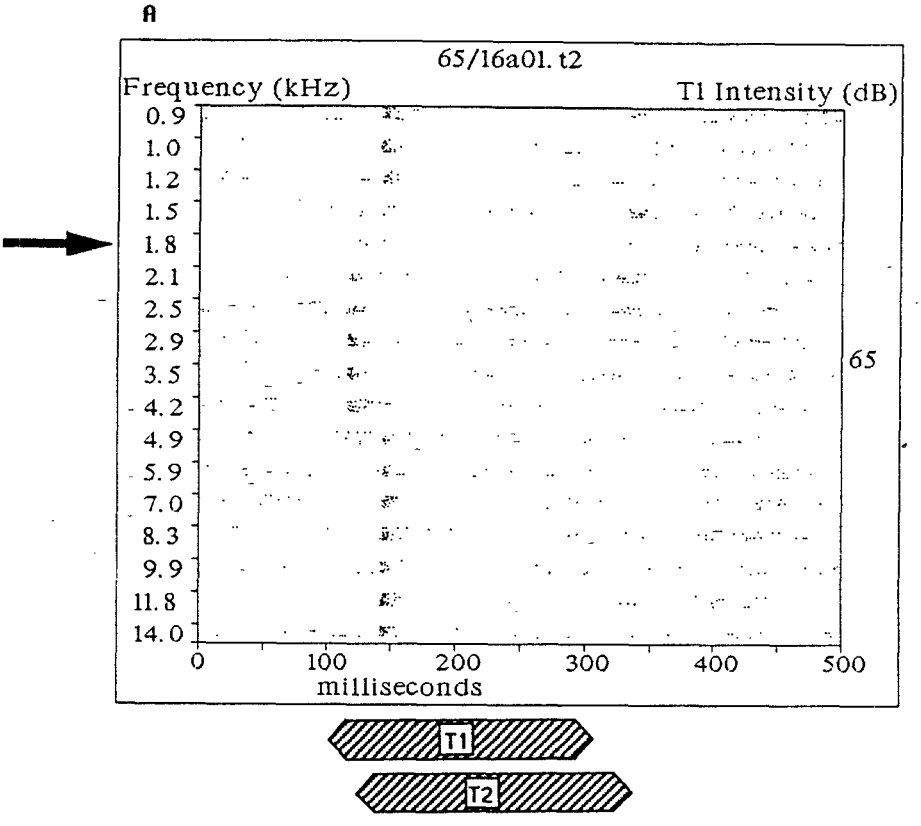
A
65/16a01.t2
Frequency (kHz)
T1 Intensity (dB)
0.9
1.0
1.2
1.5
1.8
2.1
2.5
2.9
3.5
4.2
4.9
5.9
7.0
8.3
9.9
11.8
14.0
65
0
100
200
300
400
500
milliseconds
T1
T2

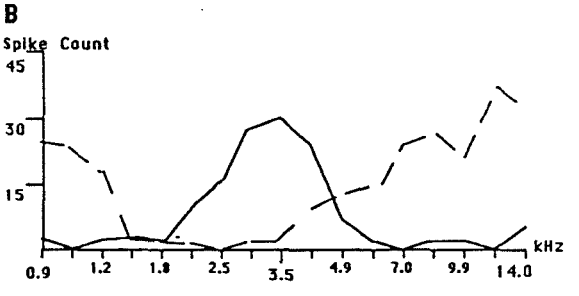
B
Spike Count
45
30
15
kHz
0.9
1.2
1.8
2.5
3.5
4.9
7.0
9.9
14.0

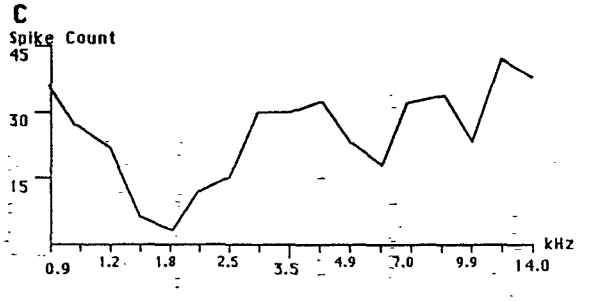
C
Spike Count
45
30
15
kHz
0.9
1.2
1.8
2.5
3.5
4.9
7.0
9.9
14.0

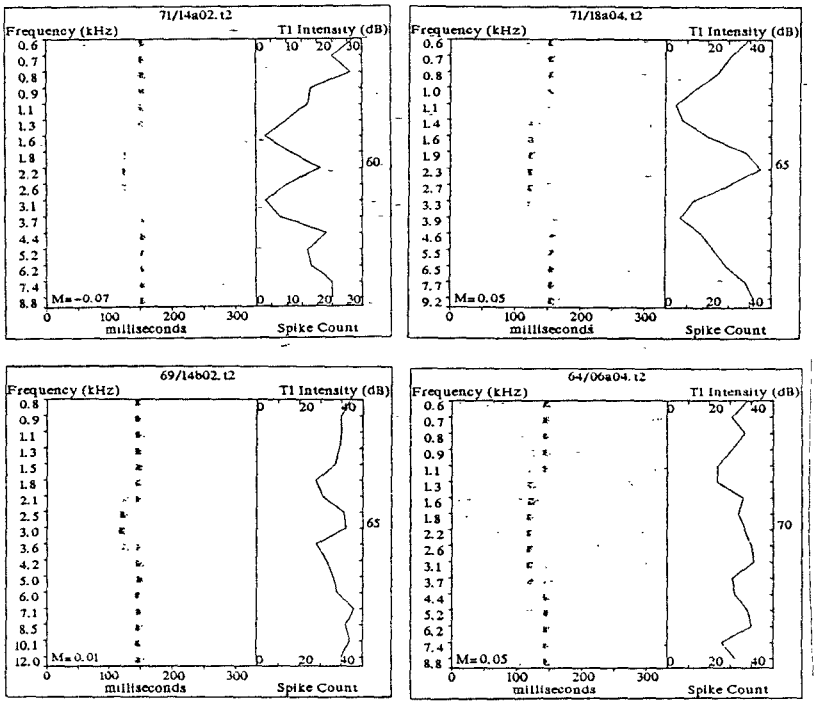
71/14a02.t2
Frequency (kHz)
T1 Intensity (dB)
0.6
0.7
0.8
0.9
1.1
1.3
1.6
1.8
2.2
2.6
3.1
3.7
4.4
5.2
6.2
7.4
8.8
M=-0.07
0
10
20
30
60
0
100
200
300
milliseconds
Spike Count
71/18a04.t2
Frequency (kHz)
T1 Intensity (dB)
0.6
0.7
0.8
1.0
1.1
1.4
1.6
1.9
2.3
2.7
3.3
3.9
4.6
5.5
6.5
7.7
9.2
M=0.05
0
20
40
65
0
100
200
300
milliseconds
Spike Count
69/14b02.t2
Frequency (kHz)
T1 Intensity (dB)
0.8
0.9
1.1
1.3
1.5
1.8
2.1
2.5
3.0
3.6
4.2
5.0
6.0
7.1
8.5
10.1
12.0
M=0.01
0
20
40
65
0
100
200
300
milliseconds
Spike Count
64/06a04.t2
Frequency (kHz)
T1 Intensity (dB)
0.6
0.7
0.8
0.9
1.1
1.3
1.6
1.8
2.2
2.6
3.1
3.7
4.4
5.2
6.2
7.4
8.8
M=0.05
0
20
40
70
0
100
200
300
milliseconds
Spike Count

Fig. 5

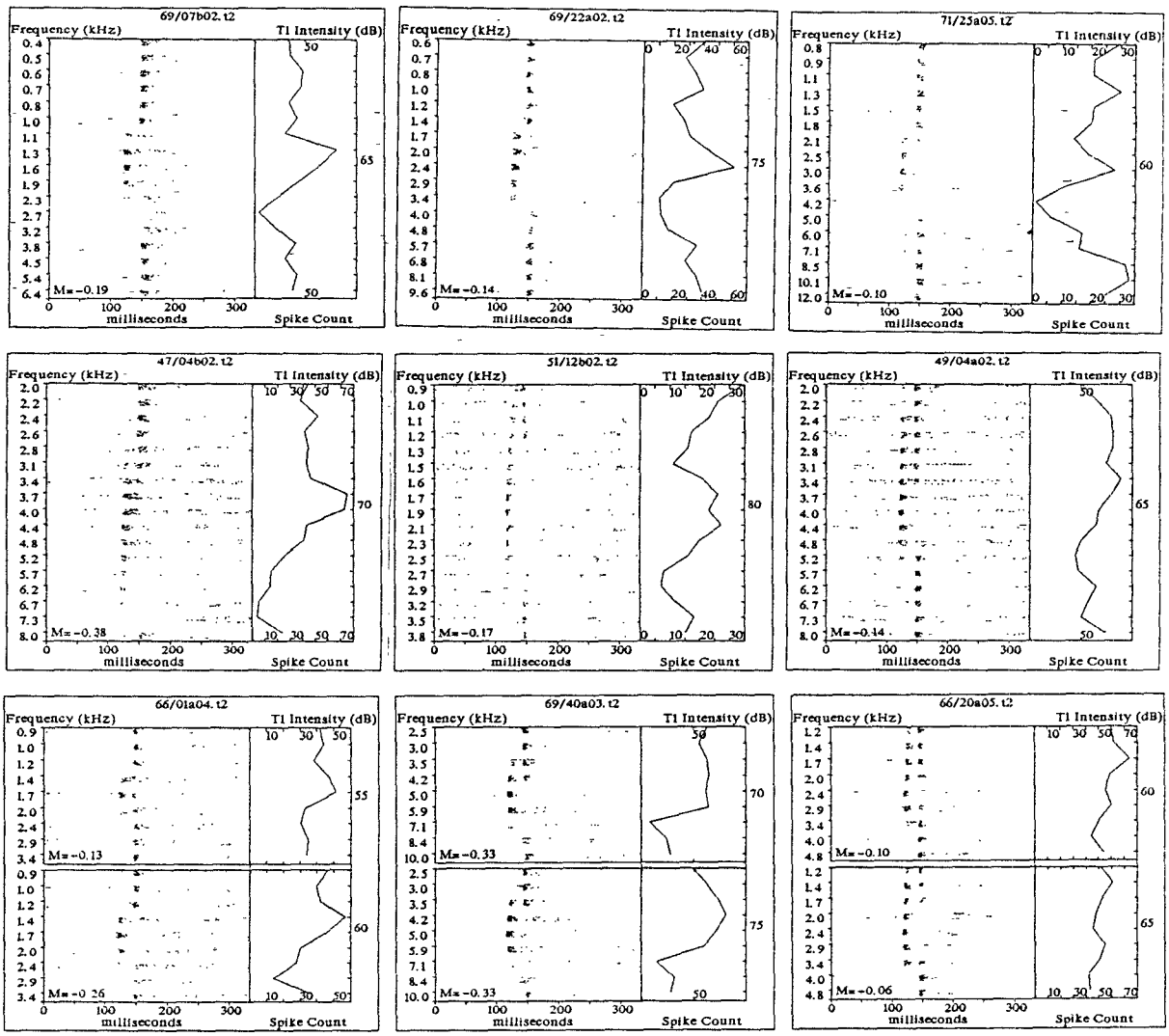
69/07b02.t2
Frequency (kHz)
T1 Intensity (dB)
M=-0.19
milliseconds
Spike Count
69/22a02.t2
M=-0.14
71/25a05.t2
M=-0.10
47/04b02.t2
M=-0.38
51/12b02.t2
M=-0.17
49/04a02.t2
M=-0.14
66/01a04.t2
M=-0.13
M=-0.26
69/40a03.t2
M=-0.33
M=-0.33
66/20a05.t2
M=-0.10
M=-0.06

Fig 6a

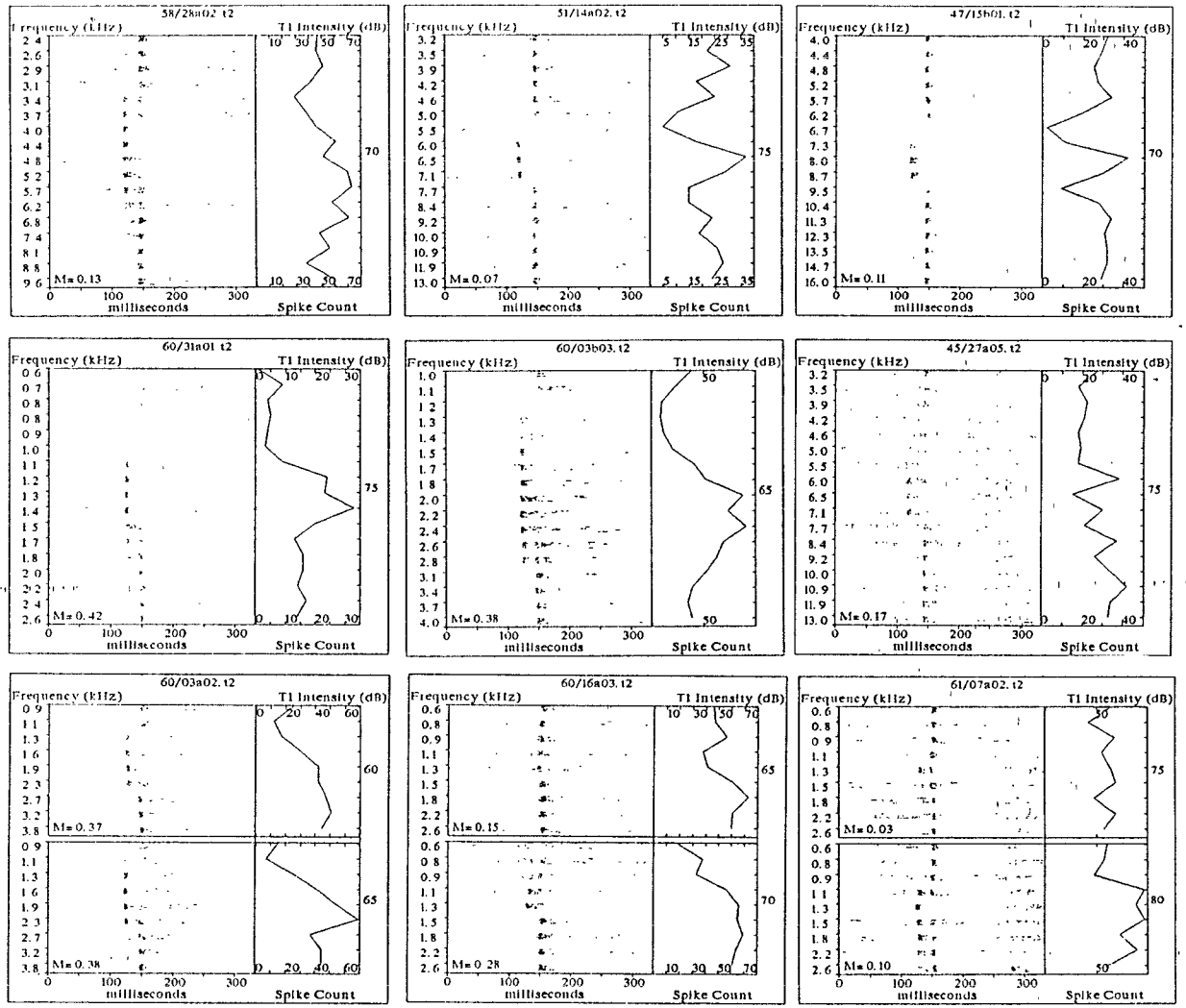
58/28a02.t2
51/14a02.t2
47/15b01.t2
60/31a01.t2
60/03b03.t2
45/27a05.t2
60/03a02.t2
60/16a03.t2
61/07a02.t2
Frequency (kHz)
T1 Intensity (dB)
milliseconds
Spike Count

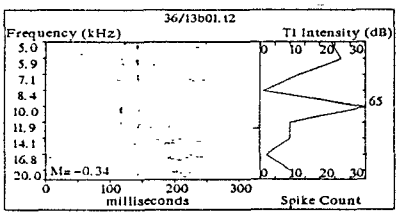
36/13b01.t2
Frequency (kHz)
T1 Intensity (dB)
5.0
5.9
7.1
8.4
10.0
11.9
14.1
16.8
20.0
M= -0.34
0 10 20 30
65
0 10 20 30
0 100 200 300
milliseconds
Spike Count

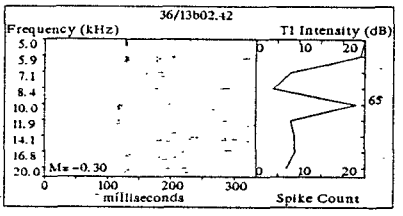
36/13b02.t2
Frequency (kHz)
T1 Intensity (dB)
5.0
5.9
7.1
8.4
10.0
11.9
14.1
16.8
20.0
M= -0.30
0 10 20
65
0 10 20
0 100 200 300
milliseconds
Spike Count

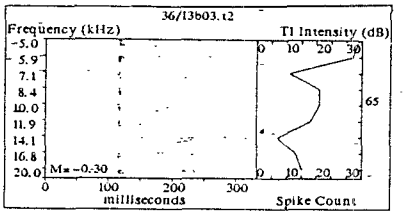
36/13b03.t2
Frequency (kHz)
T1 Intensity (dB)
5.0
5.9
7.1
8.4
10.0
11.9
14.1
16.8
20.0
M= -0.30
0 10 20 30
65
0 10 20 30
0 100 200 300
milliseconds
Spike Count

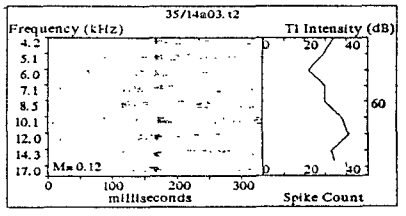
35/14a03.t2
Frequency (kHz)
T1 Intensity (dB)
4.2
5.1
6.0
7.1
8.5
10.1
12.0
14.3
17.0
M= 0.12
0 20 40
60
0 20 40
0 100 200 300
milliseconds
Spike Count

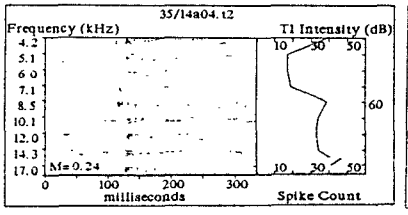
35/14a04.t2
Frequency (kHz)
T1 Intensity (dB)
4.2
5.1
6.0
7.1
8.5
10.1
12.0
14.3
17.0
M= 0.24
10 30 50
60
10 30 50
0 100 200 300
milliseconds
Spike Count

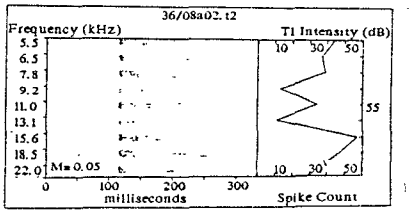
36/08a02.t2
Frequency (kHz)
T1 Intensity (dB)
5.5
6.5
7.8
9.2
11.0
13.1
15.6
18.5
22.0
M= 0.05
10 30 50
55
10 30 50
0 100 200 300
milliseconds
Spike Count

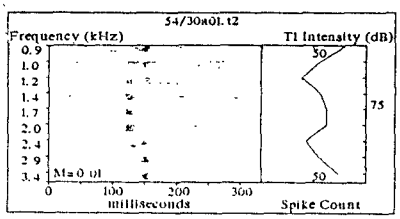
54/30a01.t2
Frequency (kHz)
T1 Intensity (dB)
M= 0.01
milliseconds
Spike Count

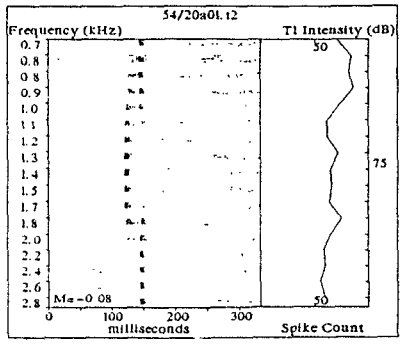
54/20a01.t2
Frequency (kHz)
T1 Intensity (dB)
M=-0.08
milliseconds
Spike Count

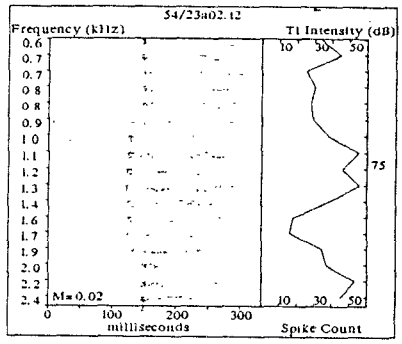
54/23a02.t2
Frequency (kHz)
T1 Intensity (dB)
M=0.02
milliseconds
Spike Count

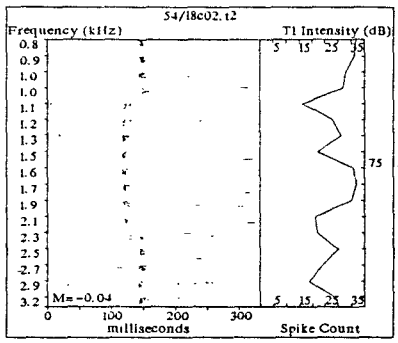
54/18c02.t2
Frequency (kHz)
T1 Intensity (dB)
M=-0.04
milliseconds
Spike Count

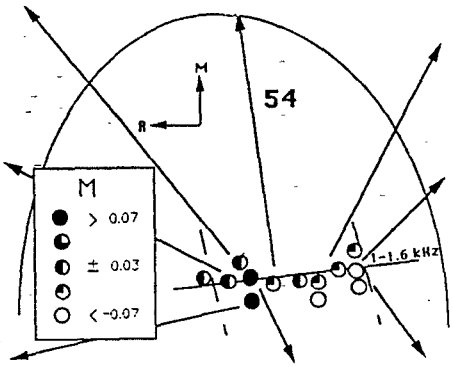
M
R
54
M
> 0.07
± 0.03
< -0.07
1-1.6 kHz

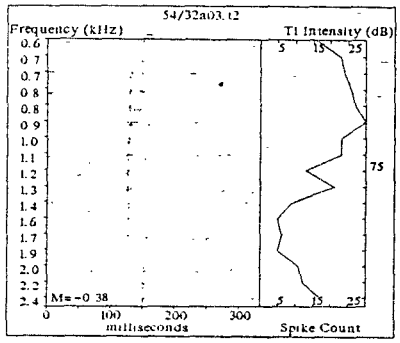
54/32a03.t2
Frequency (kHz)
T1 Intensity (dB)
M=-0.38
milliseconds
Spike Count

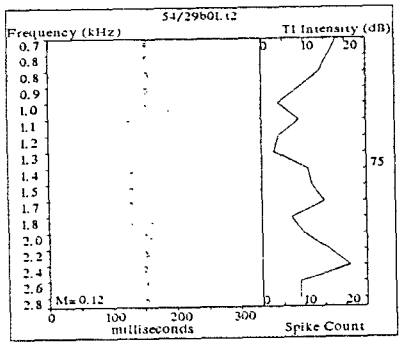
54/29b01.t2
Frequency (kHz)
T1 Intensity (dB)
M=0.12
milliseconds
Spike Count

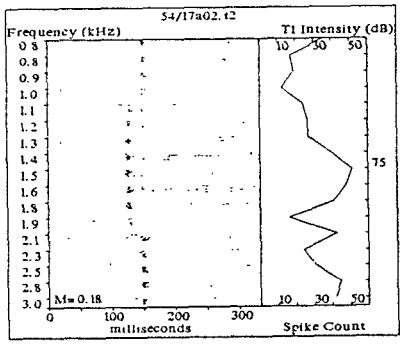
54/17a02.t2
Frequency (kHz)
T1 Intensity (dB)
M=0.18
milliseconds
Spike Count

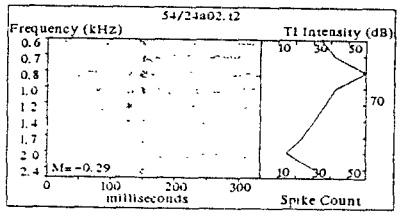
54/24a02.t2
Frequency (kHz)
T1 Intensity (dB)
M=-0.29
milliseconds
Spike Count

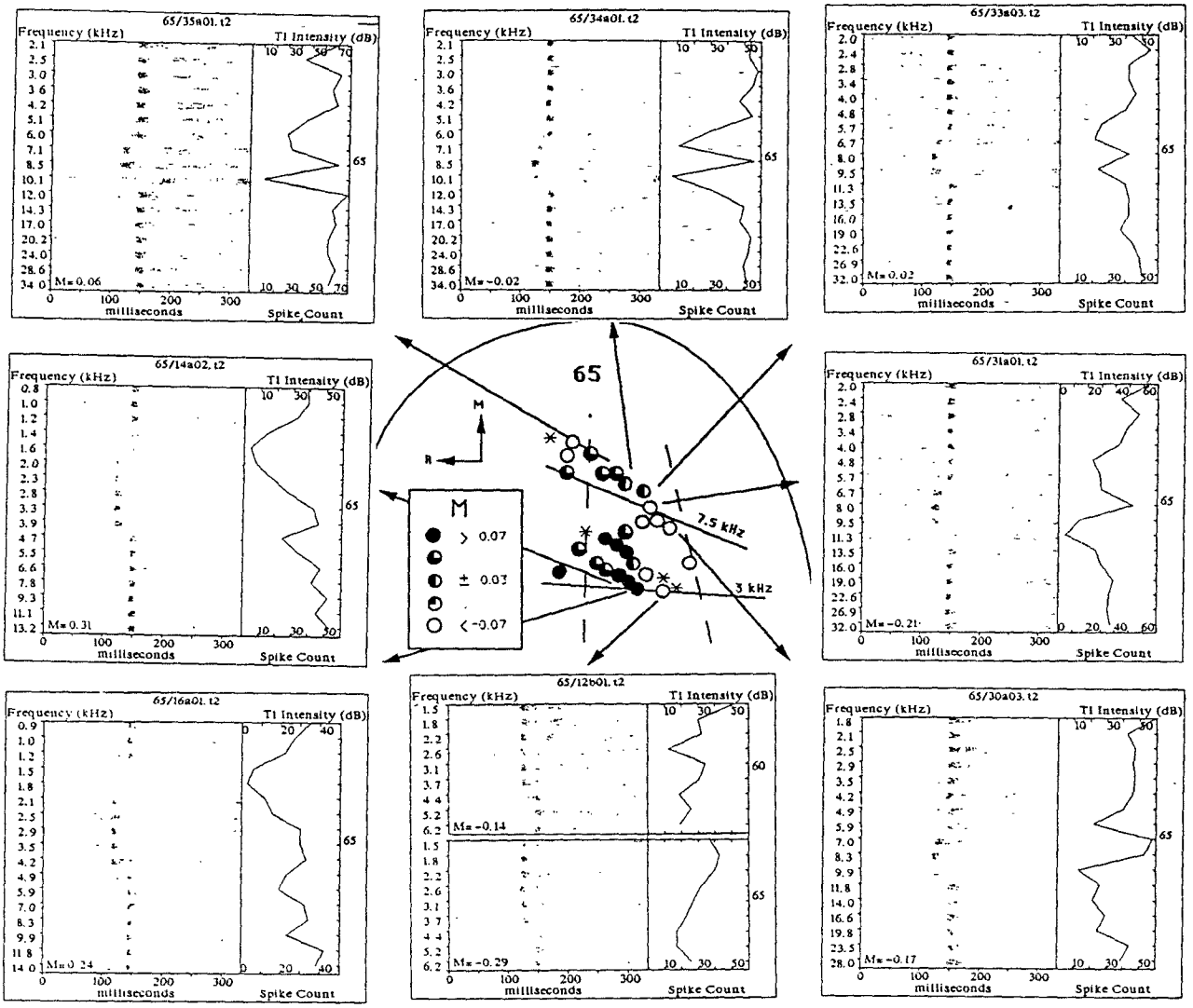
65/35a01.t2
65/34a01.t2
65/33a03.t2
65/14a02.t2
65/31a01.t2
65/16a01.t2
65/12b01.t2
65/30a03.t2
Frequency (kHz)
TI Intensity (dB)
milliseconds
Spike Count
65
M
R
7.5 kHz
3 kHz
> 0.07
± 0.03
< -0.07

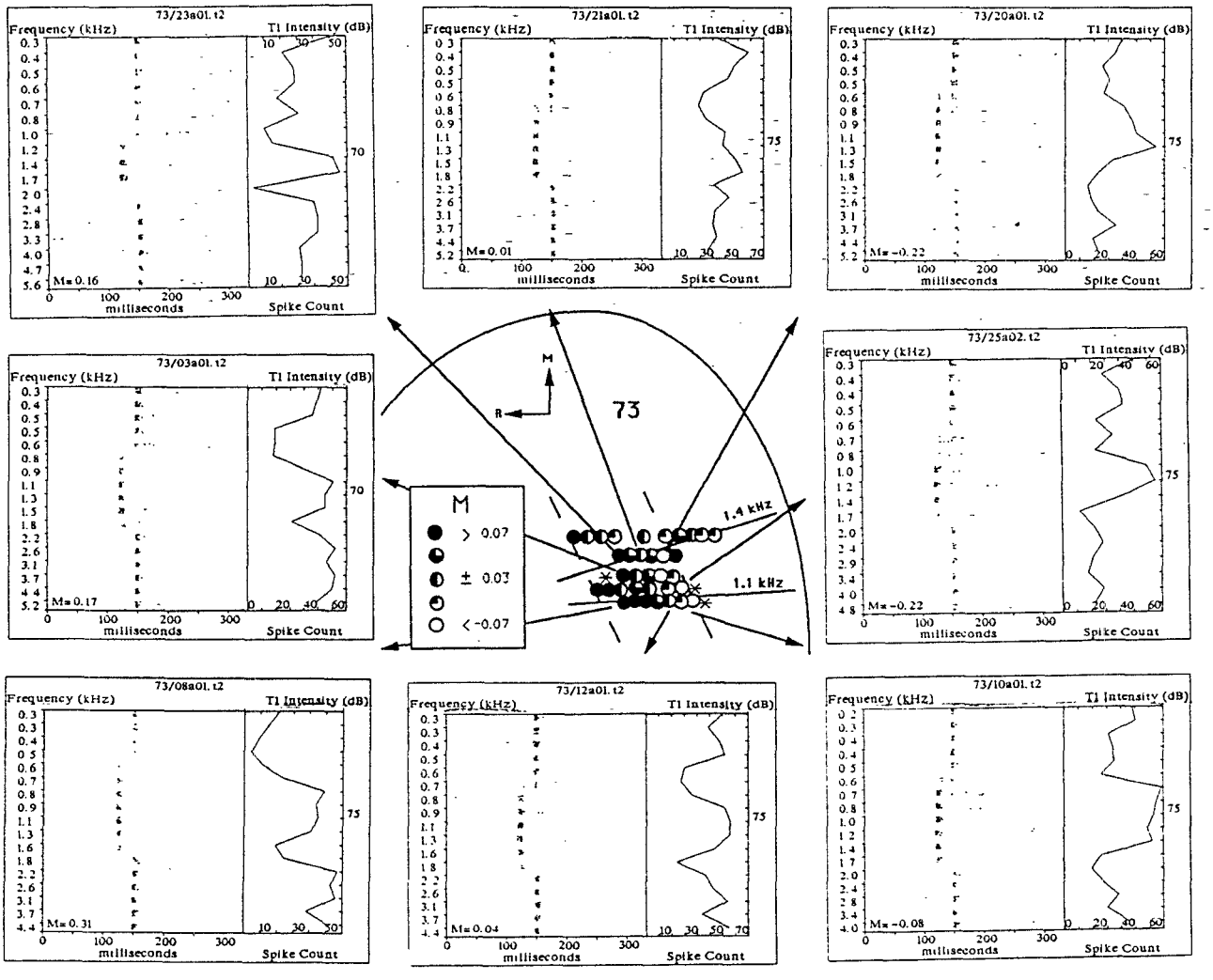
73/23a01.t2
Frequency (kHz)
T1 Intensity (dB)
M= 0.16
milliseconds
Spike Count
73/21a01.t2
M= 0.01
73/20a01.t2
M= -0.22
73/03a01.t2
M= 0.17
73
M
R
1.4 kHz
1.1 kHz
M
> 0.07
± 0.03
< -0.07
73/25a02.t2
M= -0.22
73/08a01.t2
M= 0.31
73/12a01.t2
M= 0.04
73/10a01.t2
M= -0.08

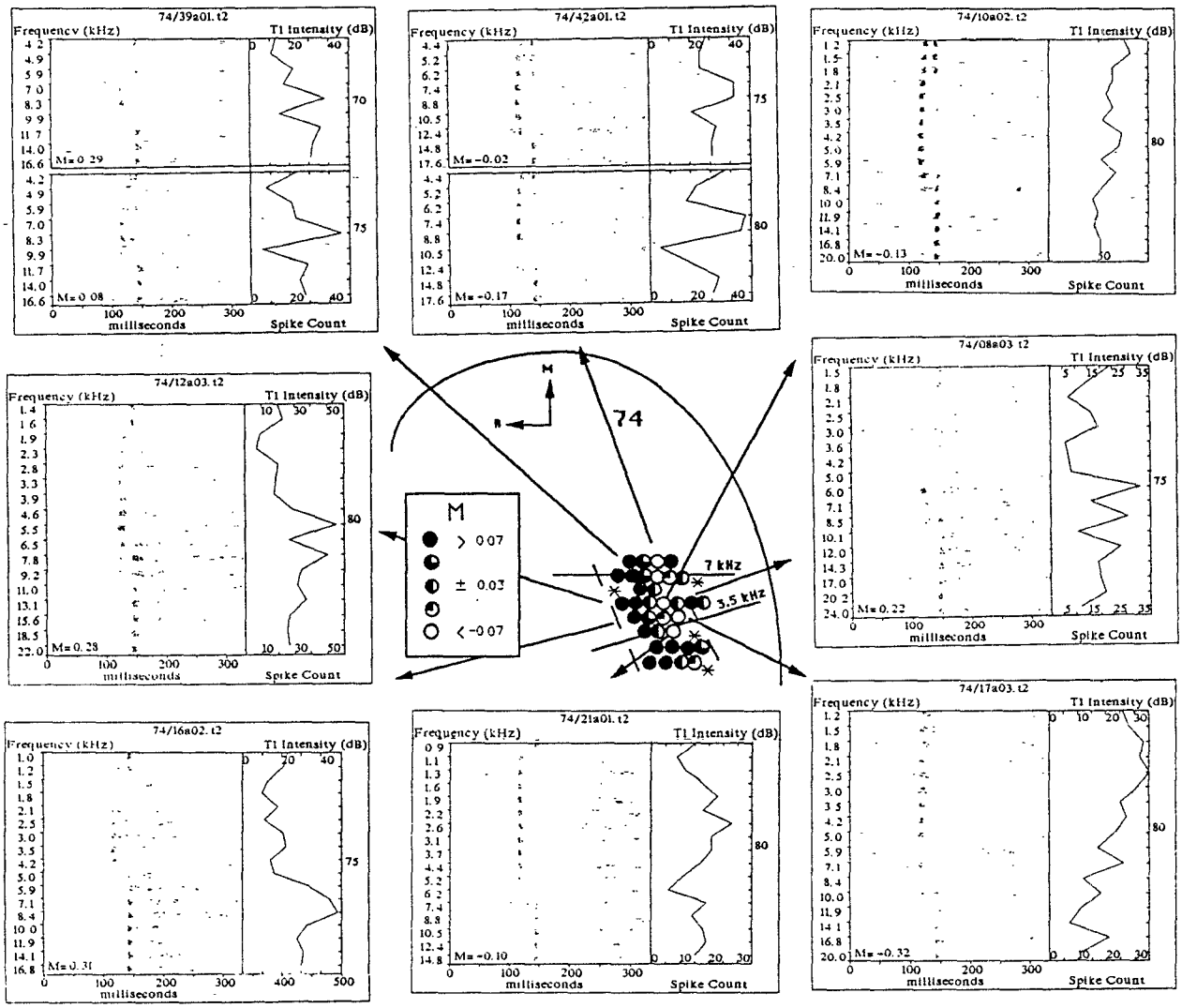
74/39a01.t2
Frequency (kHz)
T1 Intensity (dB)
M= 0.29
M= 0.08
milliseconds
Spike Count
74/42a01.t2
M= -0.02
M= -0.17
74/10a02.t2
M= -0.13
74/12a03.t2
M= 0.28
74/08a03.t2
M= 0.22
74/16a02.t2
M= 0.31
74/21a01.t2
M= -0.10
74/17a03.t2
M= -0.32
M
74
R
M
> 0.07
± 0.03
< -0.07
7 kHz
3.5 kHz

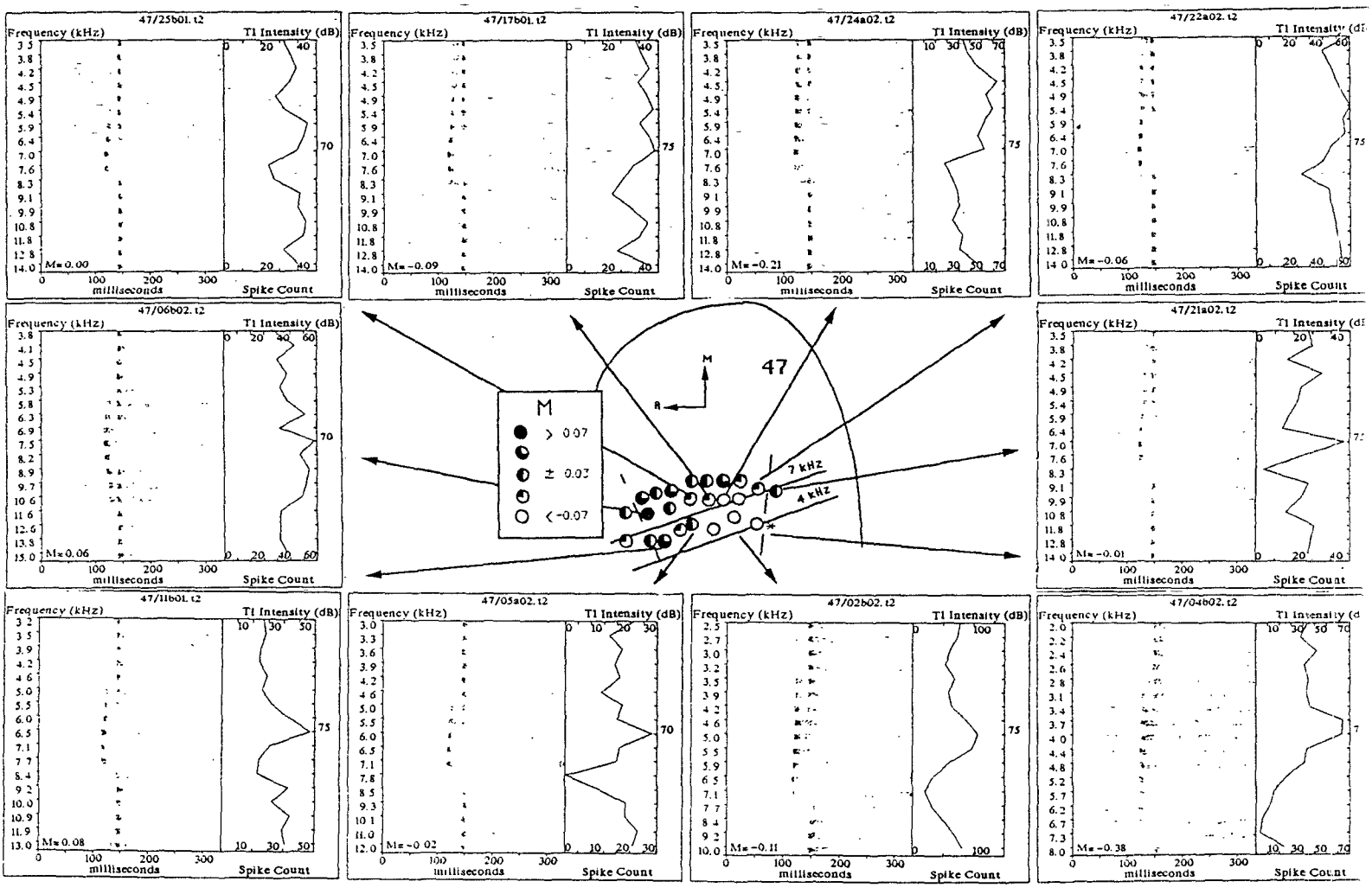
47/25b01.t2
47/17b01.t2
47/24a02.t2
47/22a02.t2
47/06b02.t2
47/21a02.t2
47/11b01.t2
47/05a02.t2
47/02b02.t2
47/04b02.t2
Frequency (kHz)
T1 Intensity (dB)
milliseconds
Spike Count
M
47
A
> 0.07
± 0.03
< -0.07
7 kHz
4 kHz

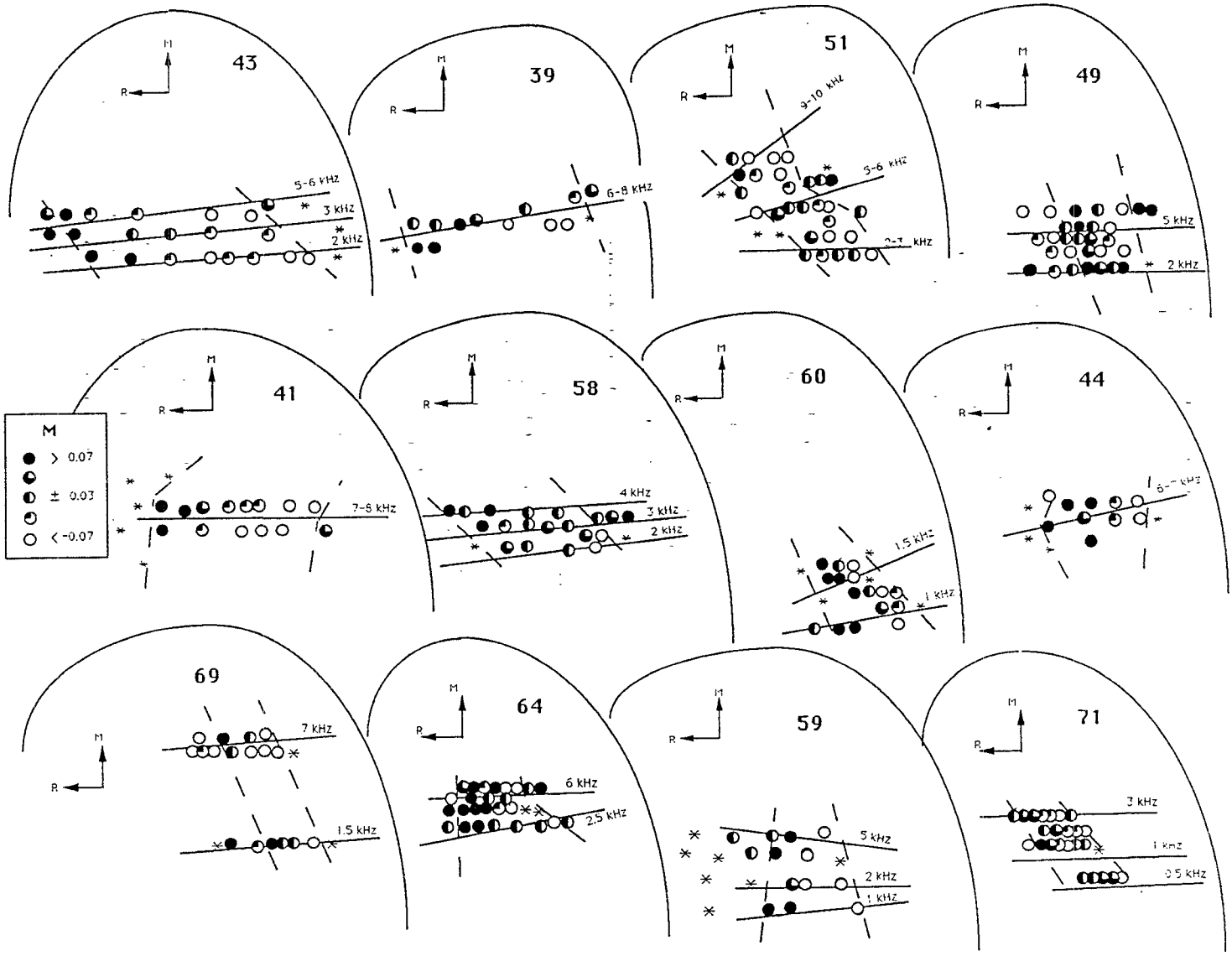
43
5-6 kHz
3 kHz
2 kHz
39
6-8 kHz
51
9-10 kHz
5-6 kHz
49
5 kHz
2 kHz
41
7-8 kHz
58
4 kHz
3 kHz
2 kHz
60
1.5 kHz
1 kHz
44
69
7 kHz
1.5 kHz
64
6 kHz
2.5 kHz
59
5 kHz
2 kHz
1 kHz
71
3 kHz
1 kHz
0.5 kHz
M
> 0.07
± 0.03
< -0.07

Fig. 1

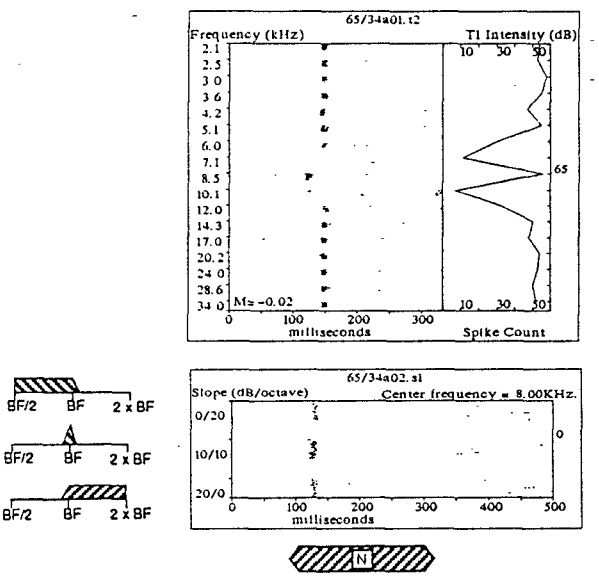
65/34a01.t2
Frequency (kHz)
T1 Intensity (dB)
2.1
2.5
3.0
3.6
4.2
5.1
6.0
7.1
8.5
10.1
12.0
14.3
17.0
20.2
24.0
28.6
34.0
10
30
50
65
Ms -0.02
0
100
200
300
milliseconds
Spike Count

65/34a02.s1
Slope (dB/octave)
Center frequency = 8.00KHz.
0/20
10/10
20/0
0
100
200
300
400
500
milliseconds

BF/2
BF
2 x BF
A
BF/2
BF
2 x BF
BF/2
BF
2 x BF

N

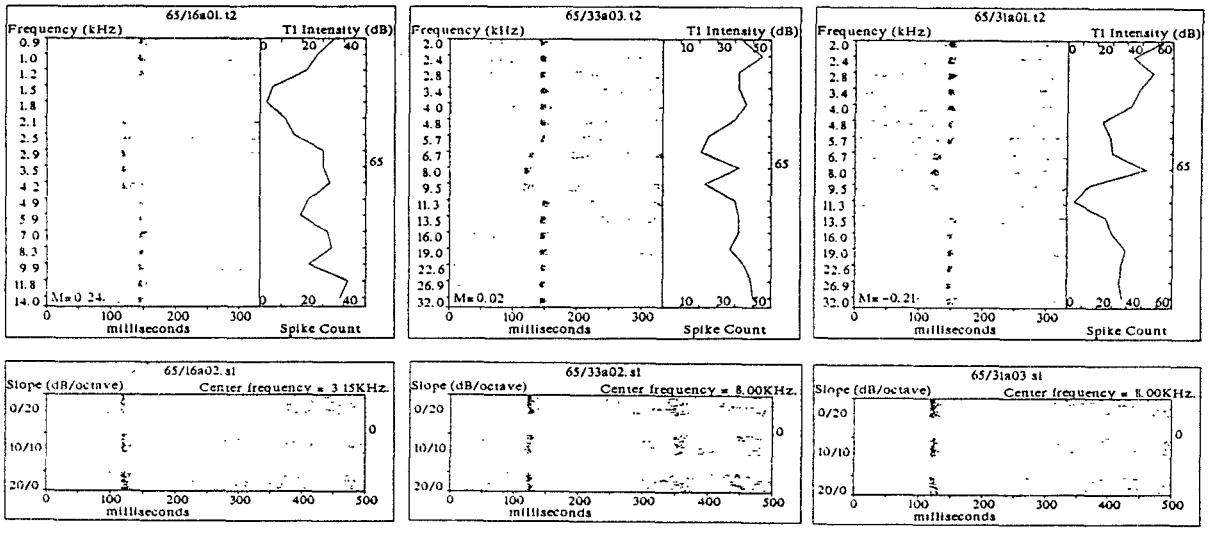
65/16a01.t2
Frequency (kHz)
T1 Intensity (dB)
0.9
1.0
1.2
1.5
1.8
2.1
2.5
2.9
3.5
4.2
4.9
5.9
7.0
8.3
9.9
11.8
14.0
M= 0.24
0
100
200
300
milliseconds
0
20
40
65
Spike Count
65/33a03.t2
Frequency (kHz)
T1 Intensity (dB)
2.0
2.4
2.8
3.4
4.0
4.8
5.7
6.7
8.0
9.5
11.3
13.5
16.0
19.0
22.6
26.9
32.0
M= 0.02
milliseconds
10
30
50
65
Spike Count
65/31a01.t2
Frequency (kHz)
T1 Intensity (dB)
2.0
2.4
2.8
3.4
4.0
4.8
5.7
6.7
8.0
9.5
11.3
13.5
16.0
19.0
22.6
26.9
32.0
M= -0.21
milliseconds
0
20
40
60
65
Spike Count
65/16a02.sl
Slope (dB/octave)
Center frequency = 3.15KHz.
0/20
10/10
20/0
0
100
200
300
400
500
milliseconds
65/33a02.sl
Slope (dB/octave)
Center frequency = 8.00KHz.
0/20
10/10
20/0
0
100
200
300
400
500
milliseconds
65/31a03.sl
Slope (dB/octave)
Center frequency = 8.00KHz.
0/20
10/10
20/0
0
100
200
300
400
500
milliseconds

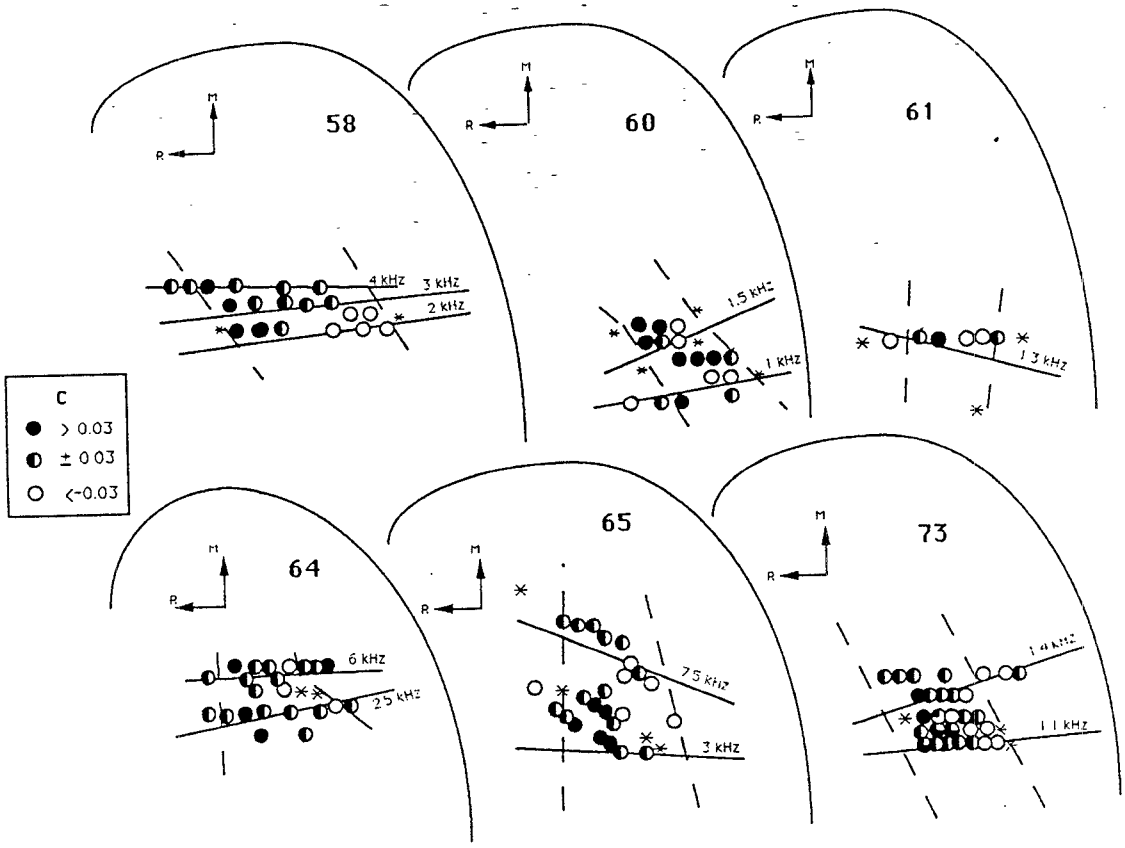
C
> 0.03
± 0.03
<-0.03
58
M
R
4 kHz
3 kHz
2 kHz
60
1.5 kHz
1 kHz
61
1.3 kHz
64
6 kHz
2.5 kHz
65
7.5 kHz
3 kHz
73
1.4 kHz
1.1 kHz

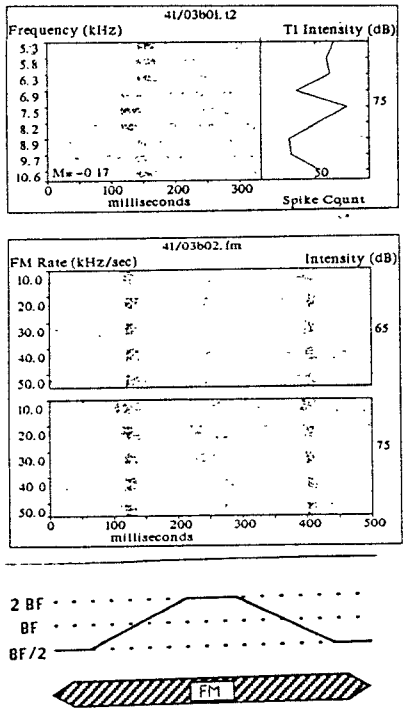
41/03b01.t2
Frequency (kHz)
T1 Intensity (dB)
5.3
5.8
6.3
6.9
7.5
8.2
8.9
9.7
10.6
M= -0 17
75
50
0
100
200
300
milliseconds
Spike Count
41/03b02.fm
FM Rate (kHz/sec)
Intensity (dB)
10.0
20.0
30.0
40.0
50.0
65
75
400
500
2 BF
BF
BF/2
FM

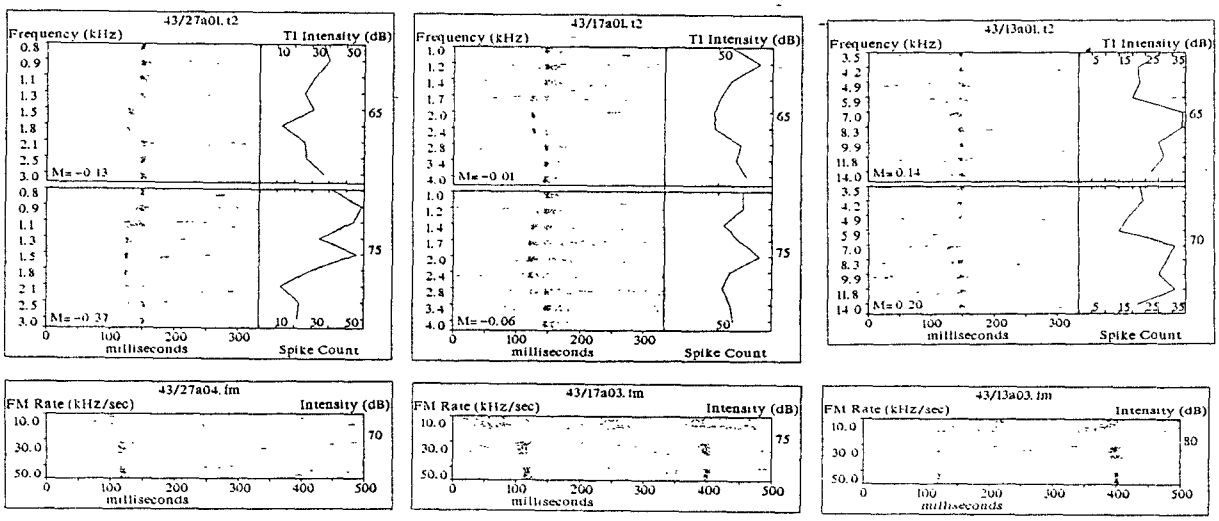
43/27a01.t2
Frequency (kHz)
T1 Intensity (dB)
M= -0.13
M= -0.37
milliseconds
Spike Count
43/17a01.t2
Frequency (kHz)
T1 Intensity (dB)
M= -0.01
M= -0.06
milliseconds
Spike Count
43/13a01.t2
Frequency (kHz)
T1 Intensity (dB)
M= 0.14
M= 0.20
milliseconds
Spike Count
43/27a04.fm
FM Rate (kHz/sec)
Intensity (dB)
milliseconds
43/17a03.fm
FM Rate (kHz/sec)
Intensity (dB)
milliseconds
43/13a03.fm
FM Rate (kHz/sec)
Intensity (dB)
milliseconds

Fig 17

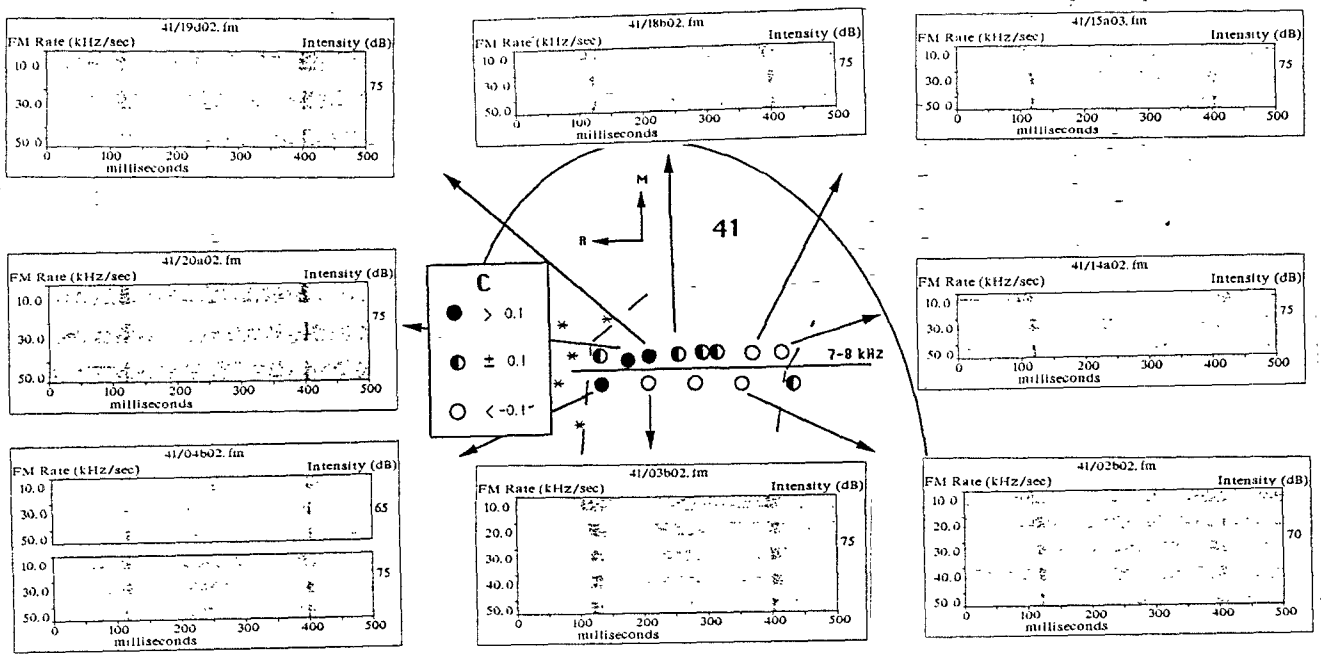
41/19d02.fm
FM Rate (kHz/sec)
Intensity (dB)
41/18b02.fm
41/15a03.fm
41/20a02.fm
41/14a02.fm
41/04b02.fm
41/03b02.fm
41/02b02.fm
milliseconds
M
R
41
C
> 0.1
± 0.1
< -0.1
7-8 kHz

Fig 18.

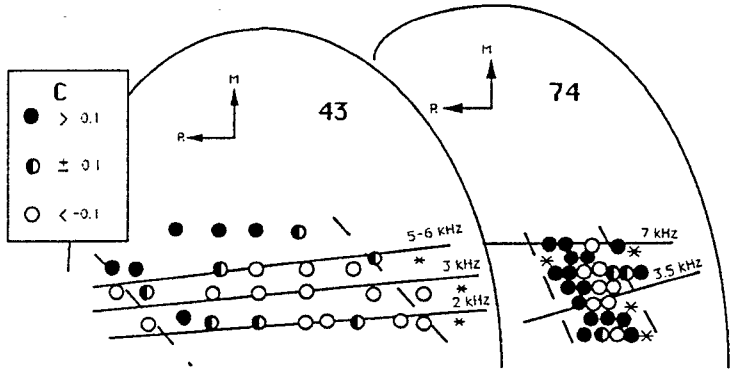
C
> 0.1
± 0.1
< -0.1
M
R
43
M
R
74
5-6 kHz
3 kHz
2 kHz
7 kHz
3.5 kHz

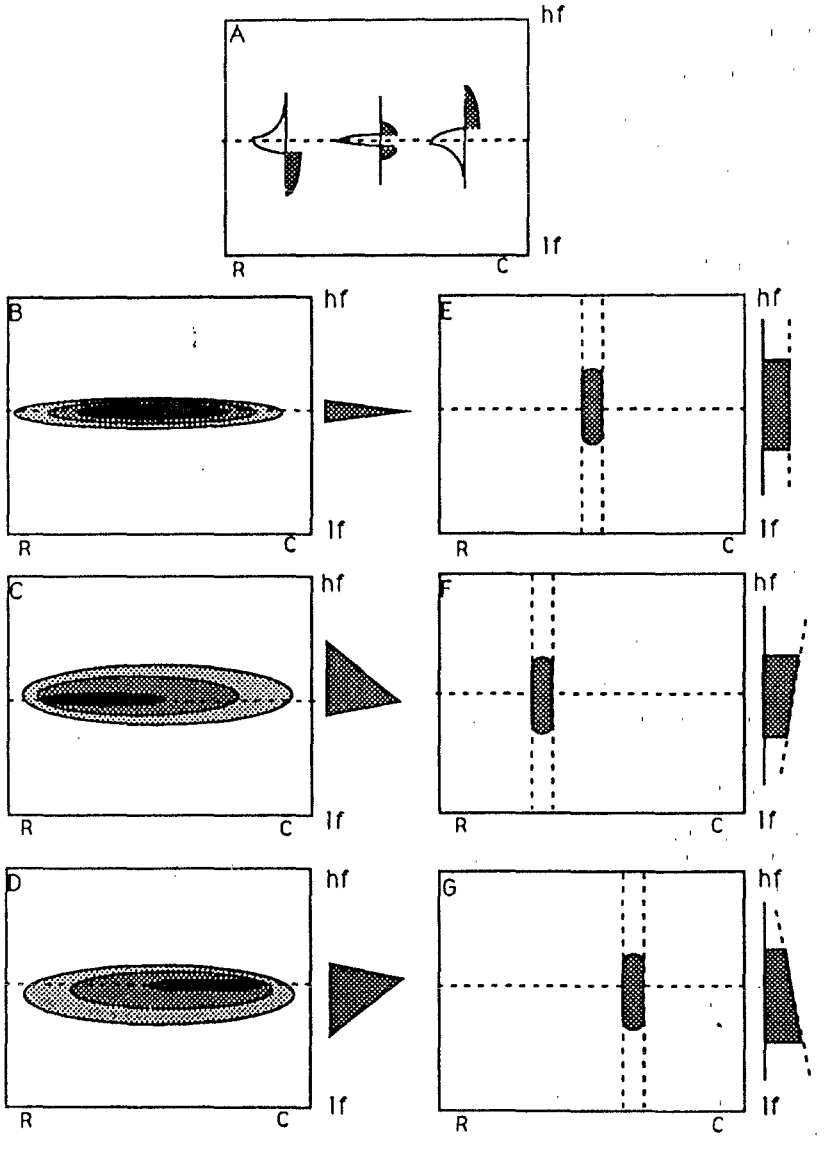
A
hf
lf
R
C
B
E
C
F
D
G

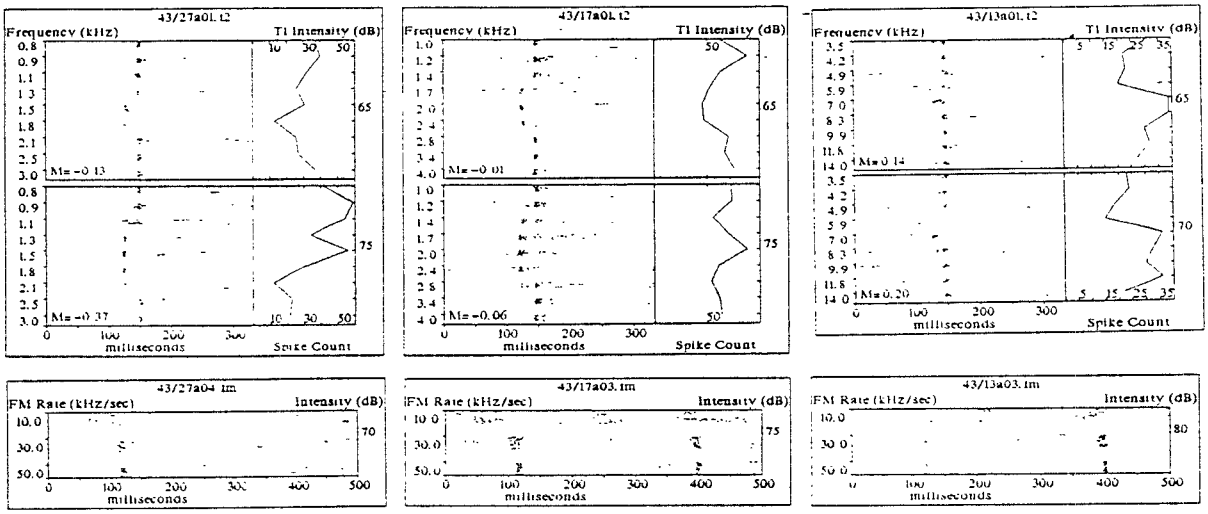
43/27a01.t2
Frequency (kHz)
T1 Intensity (dB)
Spike Count
milliseconds
43/17a01.t2
Frequency (kHz)
T1 Intensity (dB)
Spike Count
milliseconds
43/13a01.t2
Frequency (kHz)
T1 Intensity (dB)
Spike Count
milliseconds
43/27a04.tm
FM Rate (kHz/sec)
Intensity (dB)
milliseconds
43/17a03.tm
FM Rate (kHz/sec)
Intensity (dB)
milliseconds
43/13a03.tm
FM Rate (kHz/sec)
Intensity (dB)
milliseconds

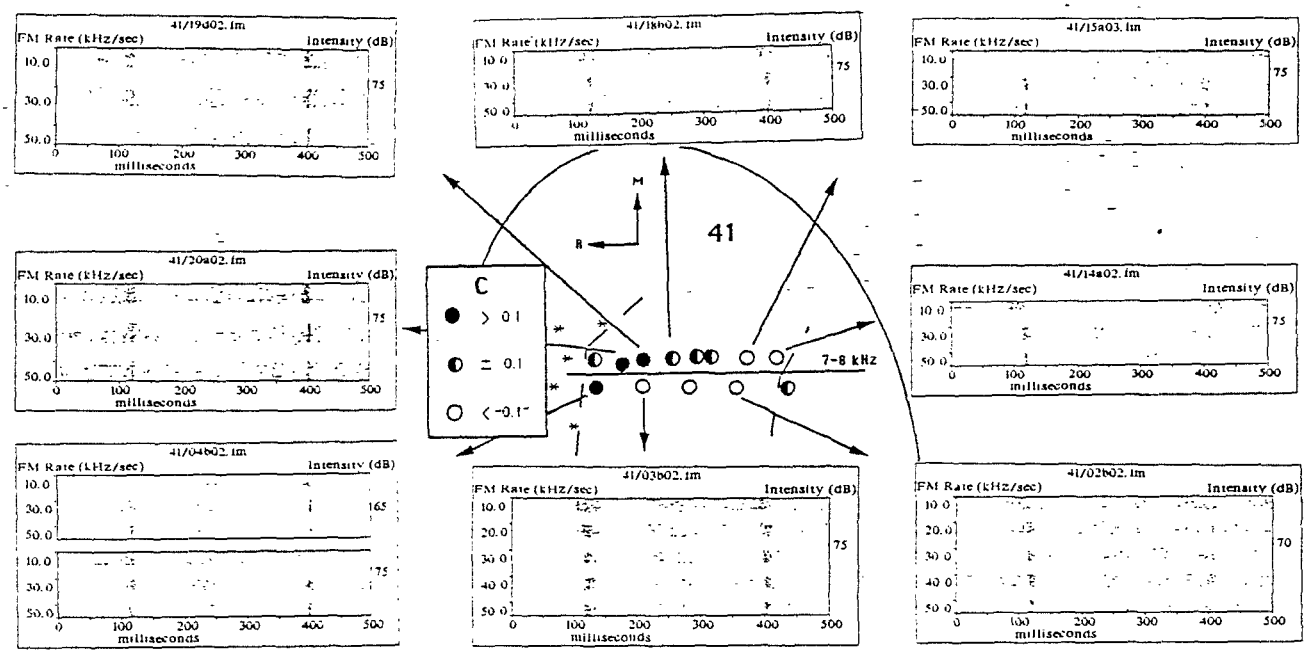
41/19d02.fm
41/18b02.fm
41/15a03.fm
41/20a02.fm
41/14a02.fm
41/04b02.fm
41/03b02.fm
41/02b02.fm
FM Rate (kHz/sec)
Intensity (dB)
milliseconds
41
M
R
C
> 0.1
= 0.1
< -0.1
7-8 kHz

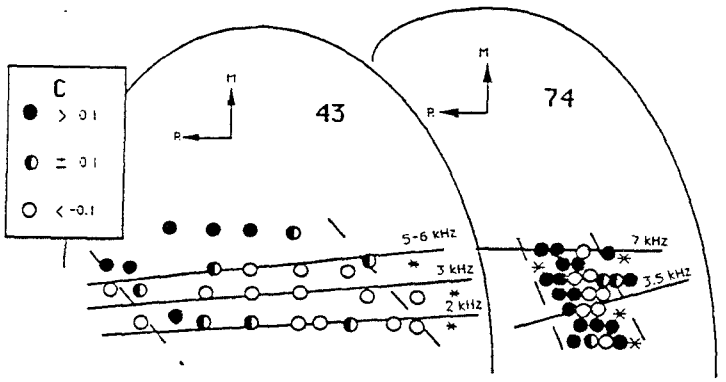
C
> 0.1
= 0.1
< -0.1
M
R
43
M
R
74
5-6 kHz
3 kHz
2 kHz
7 kHz
3.5 kHz

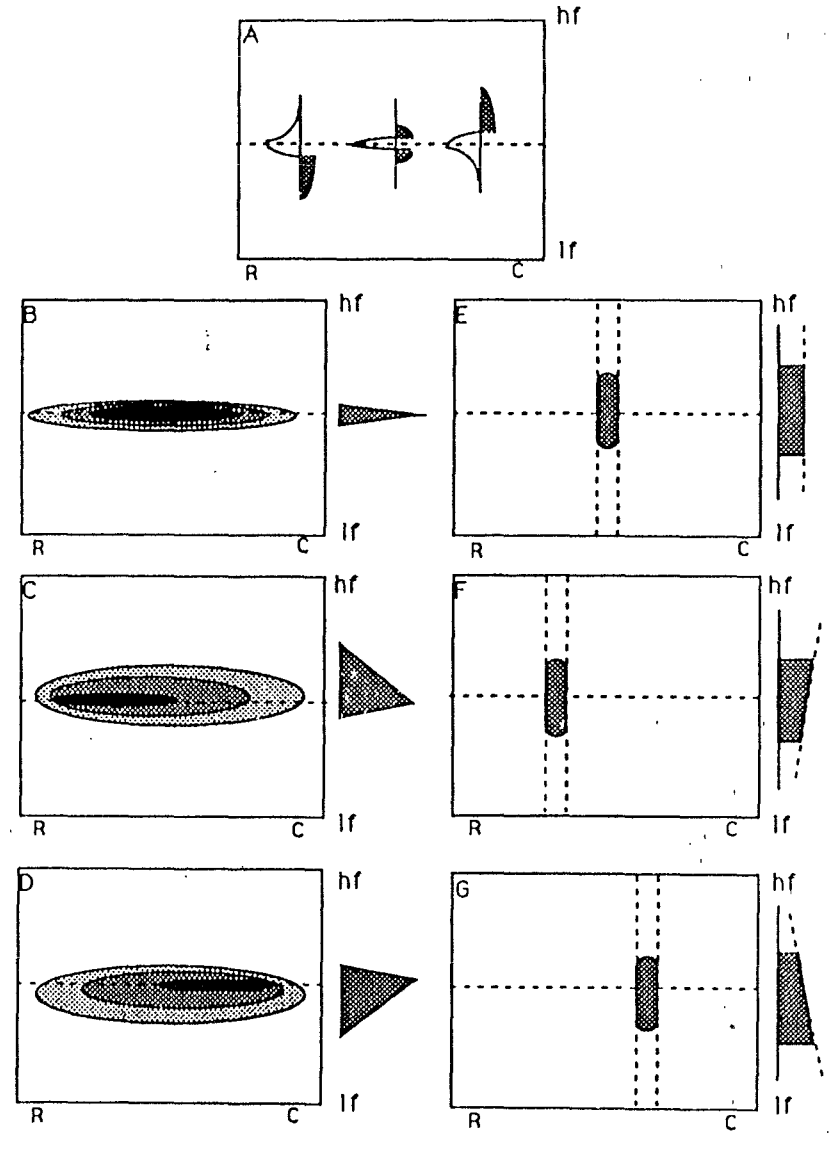
A
hf
lf
R
C
B
hf
lf
R
C
E
hf
lf
R
C
C
hf
lf
R
C
F
hf
lf
R
C
D
hf
lf
R
C
G
hf
lf
R
C